A SIMPLIFIED MODEL FOR ANGLO PLATINUM'S CONTINUOUS SECONDARY LEACH IN THE BASE METALS' REFINERY

DEBORAH ERASMUS
BLRDEB002

March 2010

Thesis submitted in partial fulfillment of the requirements of Master of Science in Engineering

ABSTRACT

An Excel-based mathematical model simulating the Base Metal's Refinery Secondary Leach operation is developed in this thesis. Fundamental building blocks of batch leach data, equipment specifications, process conditions and feed characteristics are used to develop the model. The aim of which is to develop a tool to verify actual plant performance against theoretical performance and assist with troubleshooting in the plant or serve as a basis for future autoclave design. In the present study the model is specifically used to investigate the cause of the reduced leach efficiencies that the plant is experiencing. The model utilises batch data from 2 separate test campaigns to derive kinetic parameters for the leach. The predominantly copper feedstock to the leach is approximated to chalcocite, and after analysing the batch data, the particle reaction mechanism is approximated to a shrinking core model with the rate-determining step being the chemical reaction.

Various methods for setting up the mathematical model for CSTRs are investigated and the population balance model has been selected. Two methodologies are used to solve the population balance equations derived, one solving the attained differential equation in a step-through method and the second one integrating the differential equation and solving numerically using Simpson's rule. The two models were compared to actual plant data. The correlation between the models is good, with copper recoveries varying by 0.7-1.2% and the correlation between the actual plant data and the models is fair with copper recoveries varying by 0.4-4.3%.

The use of the Rosin-Rammler-Sperling-Bennett (RRSB) equation to approximate the feed particle size distribution (PSD) is shown to be inaccurate, specifically when the solids exhibit anything other than a unimodal distribution. Using actual plant data from 2009, which exhibited a bimodal PSD and using cubic spline interpolation to model the distribution, the overall copper recovery attained is 3% lower than that obtained when the RRSB approximation is used.

The bimodal PSD that the feed material currently exhibits is not a cause of the reduced leach efficiencies. Agitator configuration, on the other hand, significantly affects copper recovery, specifically when Lightnin A315 type impellers are used instead of the 6-bladed Rushton turbine type in the first two autoclave compartments, where most of the oxidation occurs.

DECLARATION

I declare that all work, except where acknowledged, is my own.

_____

D. L. Erasmus

TABLE OF CONTENTS

List of Figures

List of Tables

ABBREVIATIONS

BMR	Base Metals Refinery
PMR	Precious Metals Refinery
RBMR	Rustenburg Base Metals Refinery
MC	Magnetic Concentrator
ACP	Anglo Platinum Converting Process
SCF	Slag Cleaning Furnace
PGM	Platinum Group Metals
DIM	Double Integrated Micromodel
MCI	Multiple Convolution Integral
SFM	Segregated Flow Model
SCM	Shrinking Core Model
PBM	Population Balance Model
CSTR	Continuous Stirred Tank Reactor
NCM	Nickel-copper Matte
PLR	Primary Leach Residue
PSD	Particle Size Distribution
RTD	Residence Time Distribution
SEM	Scanning Electron Micrograph
NSM	Numerical Simpson's Method
STM	Step-Through Method
XRD	X-Ray Diffraction

NOMENCLATURE

a	gas-liquid interfacial area per unit volume	m^2/m^3
a	stoichiometric coefficient for A	
b	stoichiometric coefficient for B	
$\overline{B}$	birth rate function	
$[B]_t$	concentration of B at residence time t	
$[B]_f$	concentration of B in feed	
C_A^s	concentration of A at surface of B	mol/m^3
C_A^{sat}	saturated concentration of A	mol/m^3
C_A^{bulk}	bulk concentration of A in solution	mol/m^3
C_A	bulk concentration of A in solution	mol/m^3
c_{aq}	aqueous molal concentration of oxygen	mol/kg
$(c_{aq})_I$	aqueous concentration of oxygen in an ionic solution	
C_I	molal concentration of ionic species	
C_G	gaseous concentration	mol/m^3
C_L	aqueous concentration of gas	mol/m^3
$\overline{D}$	death rate function	
D	diffusivity coefficient	
$D*$	normalising particle size	
D	agitator blade diameter	
E	angular coefficient of the saturation curve	
Ea	activation energy	KJ/mol
$E(t)$	residence time distribution	
F_f	molar concentration of mineral in the reactor	
$f_{0,n}(l_{0,n})$	normal distribution representing probability of particles in a size range	
$f(l)$	particle size mass-weighted distribution function	
$f(t)$	residence time density	
$f_N(\xi)$	normalised particle size distribution of particles leaving the first tank	
G	linear shrinkage rate of particles	
$I(\theta)$	internal age distribution of particles	
J	flux	$mol/m^2/s$
k_H	Henry's constant	

k_s	surface chemical rate constant	
k_L	liquid side mass transfer coefficient	
k_G	gas side mass transfer coefficient	
K	overall mass transfer coefficient	
l	particle length (diameter)	m
L	initial particle length	m
m_B	molar flowrate of B	mol/hr
m_A	molar flowrate of A	mol/hr
$m_f(L)$	mass particle size density of feed	
m_{O_2}	molar flow of oxygen	
m_t	total gas molar flow	
m_{N_2}	molar flow of nitrogen	
$M_n^P(\theta, l_{0,n})$	mass of a single particle	
n	stoichiometric factor	
$n_i(l)$	number of particles entering reactor per unit volume	
$n_o(l)$	number of particles exiting reactor per unit volume	
N	agitator speed	
N_A	molar flow of A	mol/m³/s
N_B	no. of moles of B per particle at any time	mol
p_{O_2}	partial pressure of oxygen	
P_g	gassed power	KW
p_w	partial pressure of water	
P_T	total system pressure	
P_o	ungassed power draw	KW
Q	gas flowrate	
Q_3	cumulative PSD	
q_3	density PSD	
Q	flowrate of slurry through reactor	m³/s
$\overline{r_n^R}$	average reactor bioleaching rate	
$r_n^{'}(\theta, l_{0,n})$	particle leaching rate	

r	radius of particle	m
R	universal gas constant	J/mol/K
$\bar{t}$	mean residence time per tank	
t	time	s
T	temperature	K
V	volume of reactor stage	
V_L	volume	
V_p	volume per particle	m^3
v_j	rate of change of a specific property	
v_G	superficial gas flow	
x_{O_2}	molar fraction of oxygen	
X_B	fraction of reacted solids	
x	particle size	
x'	RRSB parameter	
x^*	GGS parameter	
$x_{\max}$	GGS parameter	
$x_{50.3}$	median diameter of log normal distribution	
X_{BN}	fraction reacted in tank N	
$X(t, L, [B]_t)$	batch conversion of particle, size L	
X	mass conversion of solid B	

Greek Symbols

τ	residence time	hr
ρ_B	molar density of B	mol/m^3
ρ_{Bmass}	mass density of B	kg/m^3
ψ	population density function	
ζ	particular value of a property	
δ	boundary layer	m
σ	standard deviation	
ϕ_{MS}	fraction of pure mineral sulphide in the ore	
ρ	fluid density	
α, β	system parameters	

1 INTRODUCTION

1.1 Process Overview

Anglo Platinum is the world's largest primary producer of platinum, producing about 2.5Moz per annum. Rock rich in platinum-group metals (i.e. platinum, palladium, rhodium, ruthenium, iridium) is mined underground and in open pits and sent to concentrator plants where milling liberates the desired minerals and through flotation a sulphide-rich phase is concentrated with which most PGMs are associated. The flotation concentrate is smelted in arc furnaces and converted in the ACP (an Ausmelt processing converter), ultimately producing a slow-cooled matte containing platinum group metals (PGMs) and base metals (mainly copper and nickel). An integral part of Anglo Platinum's platinum processing chain is thus the removal and subsequent recovery of base metals from this matte, before the PGMs are further refined in the Precious Metals Refinery (PMR). This separation of base metals from PGMs occurs in the Rustenburg Base Metals Refinery (RBMR). The process flow is illustrated in Figure 1 below:

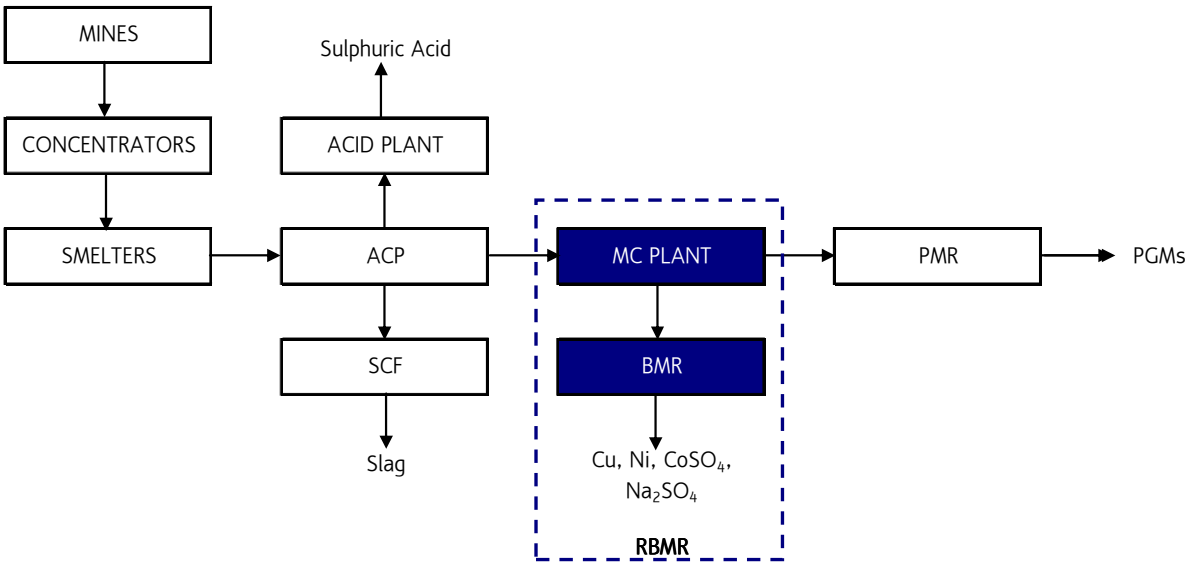

Figure 1 – A General Overview of the Anglo Platinum Processing Flowsheet

The RBMR comprises a Milling and Magnetic Concentrator Plant, where the slow-cooled matte from the ACP is milled and the resulting material is split into two streams via magnetic separators: a magnetic PGM-containing concentrate and a non-magnetic Nickel-Copper Matte (NCM). The NCM is then further processed through the Base Metals

Refinery (BMR) to produce four final products - copper cathode, nickel cathode, cobalt sulphate crystal and sodium sulphate crystal.

The simplified BMR flowsheet is shown in Figure 2:

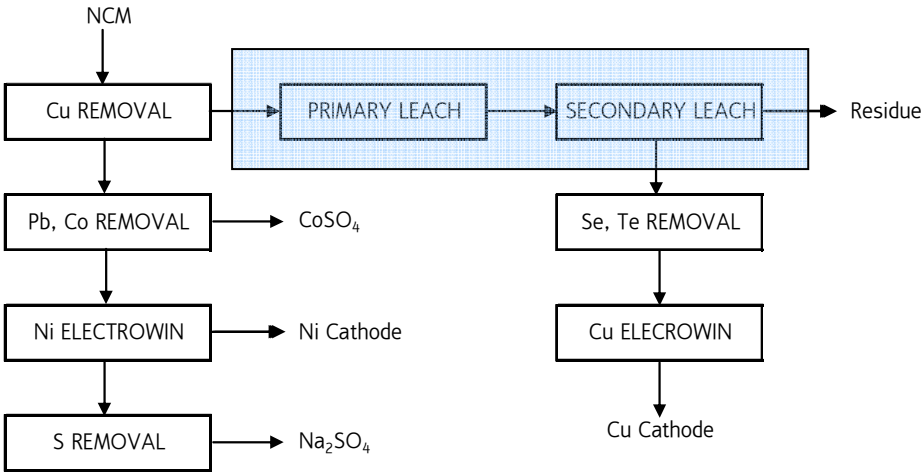

Figure 2 – The Simplified BMR Flowsheet

The heart of the base metal refining plant is the pressure leach section, comprising five continuous autoclaves utilised for primary and secondary leaching. The primary leach facilitates nickel dissolution, rejecting copper and iron into the primary leach residue (PLR) stream, which acts as the feedstock for the secondary leach. The secondary leach has three functions [1]:

- Copper extraction – the PLR solids (containing >50% copper) are leached in the secondary autoclaves, which allows for final copper recovery via electrowinning further downstream;
- Iron removal – by precipitation of the iron into the secondary leach residue as a hematite or jarosite;
- Removal of impurities (like selenium, tellurium, arsenic) – collected into the iron rich residue to ensure that the BMR products (specifically nickel cathode, copper cathode, cobalt sulphate crystal and sodium sulphate crystal) meet their required grade specifications.

1.2 Equipment

The secondary leach autoclaves are each 80m^3, four compartment, mild-steel, brick lined vessels that were originally designed by Sherritt Gordon. They are 13m long with a

diameter of 3.5m. Each compartment houses an air sparger to supply either enriched or compressed air to the slurry, and an agitator to suspend the solid particles and facilitate mass transfer of oxygen for the leach reactions. While each compartment can be supplied with steam for heating, only the second and third compartments have cooling coils [2]. A schematic of one of the autoclaves is shown in Figure 3:

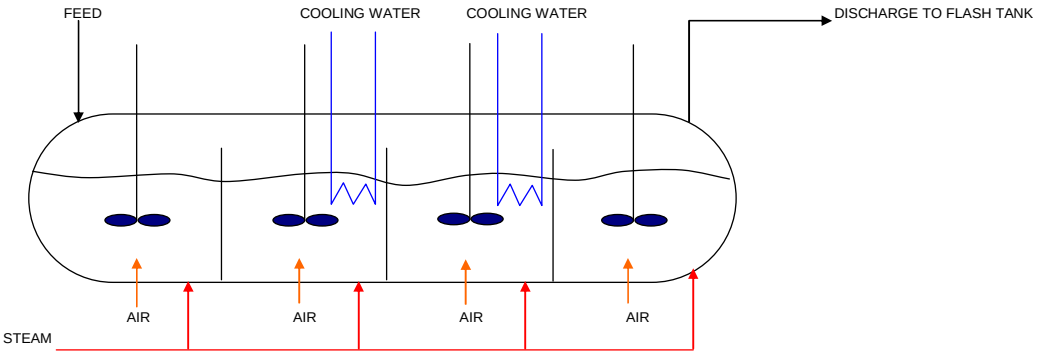

Figure 3 – Secondary Autoclave Schematic

There are three autoclaves that can perform secondary leach duty: two of these are reserved solely for secondary leaching (referred to as Secondary 1 and 2) and a third acts as a standby 'dual' autoclave that can either operate under primary leach conditions or secondary leach conditions. During 1993 the BMR expanded the secondary leach capacity by converting the autoclaves to operate on enriched air (28-34% oxygen), and not only on compressed air [1]. Secondary 1 and 2 were retrofitted entirely with Lightnin A315 (A) aerofoils (to provide good gas dispersion) and so their configuration is A-A-A-A. The dual autoclave's 3rd and 4th compartments were fitted with A315s, but Rushton's (R) were retained in compartments 1 and 2 as primary leach conditions require no gas dispersion in the 3rd and 4th compartments [1]. The dual autoclaves agitator configuration is thus R-R-A-A. The two types of agitators used in the autoclaves viz. the 6-blade Rushtons and Lightnin A315s are shown below in Figure 4.

Figure 4 – Rushton and A315 Agitators used in the Secondary Leach Autoclaves

2 PROBLEM STATEMENT, HYPOTHESIS AND APPROACH

Anglo Platinum started to experience poor leach efficiency in the secondary leach circuit during 2008, where the copper recovery in the leach decreased from ~96-98% to about 80%. An in depth investigation into this phenomenon was initiated, and part of the investigation involved batch leach tests conducted at Anglo Research Laboratories. The batch tests, however, showed that the material leached well, indicating that the problem was most likely not related to reaction kinetics, but rather with the operating parameters of the process. It also indicated that interpretation of batch leach data for a continuous leach operation is not straightforward. The equipment specifications, in particular the agitator type and configuration were then investigated, as it is well known that oxygen mass transfer is a potential limitation in the oxidative leaching of copper. Investigation of the autoclave operational parameters involved analysing the particle size distribution (PSD) of the feed material, which was found to differ from that reported in historic data, with a larger portion of coarser particles present.

It was therefore postulated that the reduced leach efficiency experienced in the autoclave is attributable to either reduced mass transfer efficiency through a changed agitator configuration and/or due to a changed particle size distribution of the feed.

As there was no option to test this hypothesis experimentally on a full scale production autoclave, it was decided to explore it through an appropriately developed and calibrated model. As there was no existing continuous leach model available to plant metallurgists, it was decided to systematically develop such a model, not only to specifically investigate the hypothesis stated above, but also to create a tool with which to analyse operational plant data on an ongoing basis.

The objective of this project is thus to develop a simple Excel-based mathematical model, based on the following fundamental building blocks:

- Batch leach results
- Equipment specifications
- Process conditions (such as temperature and air flowrate)
- Feed characteristics (such as chemical composition and particle size)

The key use for this model is to describe the continuous leaching operation of the BMR's secondary leach, in order to analyse current plant operation, either by verifying actual plant performance against theoretical performance, or by determining the effect of varying operating conditions to pinpoint problem areas or options for optimisation. The model can furthermore serve as a basis for the preliminary design of future continuous leach operations within Anglo Platinum.

The approach taken in this study was to investigate available modeling approaches in the literature and those previously pursued internally at Anglo Platinum, select the simplest and most appropriate methodology, develop a simple leaching modeling tool that can be used by plant personnel, evaluate the model predictions against operational data to prove it is meaningful and then specifically investigate the effect of PSD and agitator type and configuration on leach recovery to ascertain if either of these are responsible for the poor secondary leach efficiency.

3 LITERATURE REVIEW

The leaching of mineral particles within an aqueous solution is complex, and the analysis of the leaching process must account for the many factors involved. These include changes in the solid particles as the desired minerals are leached into solution, changes in temperature and pressure, and changes in the aqueous medium such as concentration of dissolved species or density.

Peters [3] describes this modeling process - where the aim is to establish a relationship between the mineral extraction and the mean residence time in the reactor - in terms of micromodels and a macromodel. The micromodel describes the changes that occur at the surface of the particles as a result of leaching – changes in size, size distribution and shape. The simplest micromodel describes the change in the size distribution of leaching particles as material dissolves from the surface, and the particles shrink in size. The macromodel describes the macro properties for the process, like system pressure, volume changes, temperature changes and solution composition changes. These properties are calculated using mass and energy balances.

A continuous leaching model therefore needs to incorporate macro and micro elements, and can be divided into the following four areas:

- A particle reaction model - to explain the rates of reaction and the rate determining step for the chemical reactions occurring on or within the individual solid mineral particles;
- A mathematical methodology - a model to calculate the mineral recovery attainable in a set of reactors or leach stages operating continuously;
- Mass balance equations - to calculate the change in concentration of reagents and reactants through the system of leach stages; and
- Energy balance equations - to calculate heating or cooling requirements for the system.

The first three areas (viz. particle reaction model, mathematical methodology and mass balance equations) form part of the model developed in this paper and are discussed further below.

3.1 Particle Reaction Models

Solid reactant particles can be loosely classified as porous or non-porous.

3.1.1 *Non-porous Models*

One of the most commonly used models for non-porous reactants is the Shrinking Core Model (SCM) [4], described in Figure 5, which describes the reaction of gas with particles where the overall size does not change; the reactant core shrinks over time and an "ash" layer of product is formed.

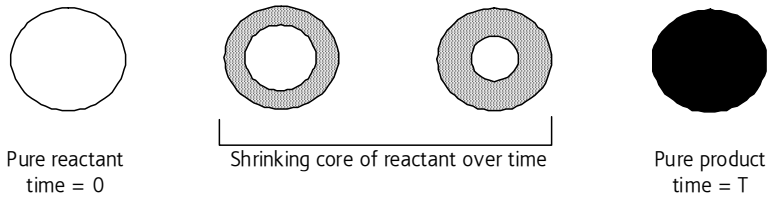

Figure 5 – Depiction of the Shrinking Core Model

Various shrinking particle models for non-porous particles have been proposed as well. Safari et al [5] summarise two additional commonly used leaching models as:

- Shrinking particle – the reactant particle shrinks over time as it reacts, with no product layer formation;

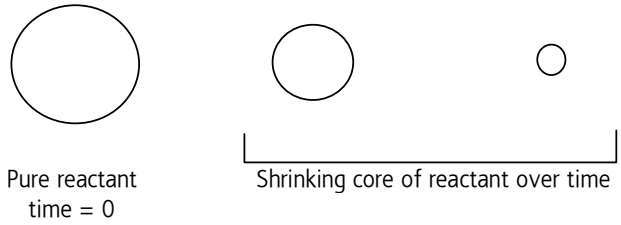

Figure 6 – Shrinking Particle Illustration

- Shrinking core-shrinking particle – the reactant forms a product layer and shrinks over time.

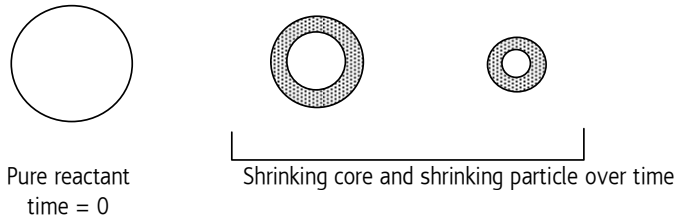

Figure 7 – Shrinking Core – Shrinking Particle Illustration

3.1.2 Porous Models

Porous particles do not have a core. For porous reactants, Levenspiel [6] describes some of the various other models, briefly summarised in Table 1:

Table 1 – Examples of Particle Models Described in Levenspiel [6]

The Uniform Conversion Model (UCM) - where uniform conversion of reactant to product occurs throughout the entire particle.	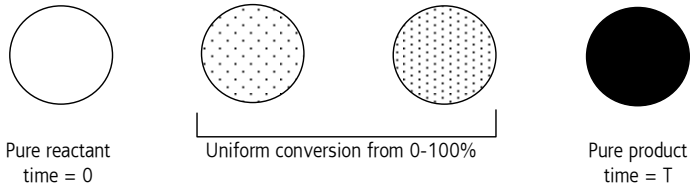
The Grainy Pellet Model (GPM) - each particle is divided into numerous sub-particles and each sub-particle reacts according to the shrinking core model.	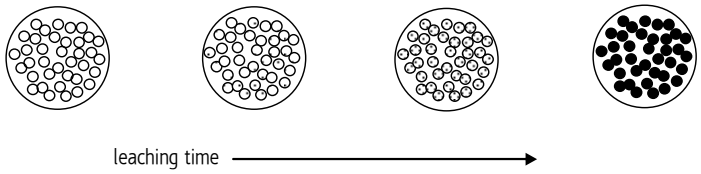
Crackling Core Model (CCM) – non-porous reactant results in a porous product, where each grain reacts according to the SCM.	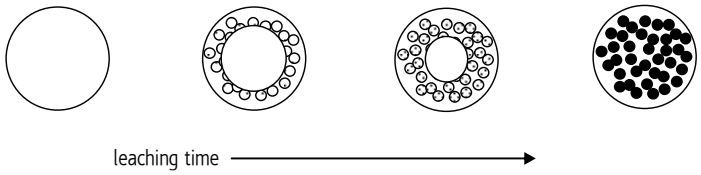
Changing Voidage Model (CVM) – an extension of the GPM, where voids in the particle increase or decrease.	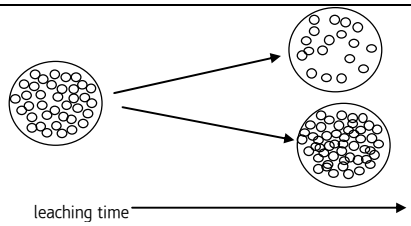

Various Thermal Decomposition Models – where the reactants are at different temperatures.	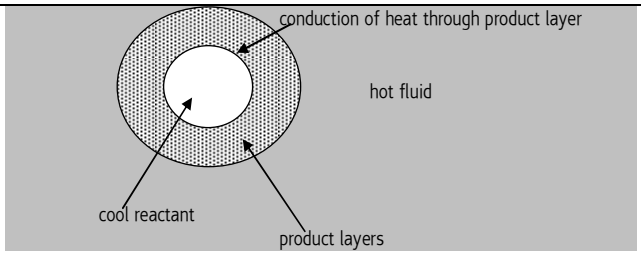

More sophisticated models exist that account for phase changes during reactions or incorporate multi-step reactions. All of the afore-mentioned models simplify the reactions that occur on the reactant particle surfaces. They do not account for variations in mineralogy that may cause different particles to react differently. As the mineralogy of the particles varies, the type of particle reaction mechanism per particle may also vary.

3.1.3 Rate Determining Step

Once the particle model has been selected, the mechanisms involved in lixiviant contacting with mineral and reacting need to be considered. The leaching of a solid particle - depending on the porosity of the particle, type of products formed, type of gas and liquid interaction with the mineral - may incorporate a number of stages (Nicol [4]), specifically:

- Mass transfer of lixiviant from the bulk solution to the surface of the particle;
- Mass transfer of products from the particle to the bulk solution;
- Mass transfer within particle pores to the reactive mineral;
- Mass transfer across product layers that may accumulate around the particle; and
- Chemical reaction at the mineral surface.

By selecting the rate determining step (the slowest step in the reaction process that determines the overall rate of the chemical process), a simplified model can be selected. In some cases a set of serial reactions occur, each with its own rate controlling mechanism.

3.2 Mathematical Leach Models

Crundwell [7] reviews the three different approaches that have been used to mathematically model leaching in Casters. He lists these methods as the Monosized Particle Model, the Segregated Flow Model and the Population Balance Model. In a separate paper Dixon and Dreisinger describe two additional models: the Doubly Integrated Micromodel [8] and the Multiple Convolution Integral [9]. Kotsiopoulos et al [10] present a Population Balance Model that incorporates the effect of particle residence time on bioleach reactor performance. Each of these models is summarised below:

3.2.1 *Monosized Particle Model*

According to Crundwell [7], this model assumes that the feed and discharge particles are all monosized. Sepulveda and Herbst [13] and Crundwell and Bryson [14] show that variances in the particle sizes at the inlet have a marked effect on the leaching model's prediction accuracy. The reason for this is that, in a train of leach reactors, the residence time distribution at each stage will result in a change in particle size distribution (PSD).

3.2.2 *Segregated Flow Model (SFM)*

The stream entering the reactor comprises separate small fluid elements and each element behaves as a batch reactor. When applying this model to leach reactors, the fundamental assumption is made that the concentration of the reactant is constant with residence time and equivalent to the exit concentration [7]. The equations to solve the SFM are:

$$1 - X = \int_0^\infty \int_0^\infty \{1 - X(t, L, [B]_t)\} m_f(L) f(t) dL dt$$

$$[B]_t = [B]_f - F_f \eta X(t, L, [B]_t)$$

where

$[B]_t$ = concentration of B at residence time t

$[B]_f$ = concentration of B in feed

F_f = molar concentration of mineral in the reactor

η = stoichiometric factor

$X(t, L, [B]_t)$ = batch conversion of particle, size L

$m_f(L)$ = mass particle size density of feed

$f(t)$ = residence time density

However, if the reactant is consumed in sufficient quantities (so that $[B]_t$ is not constant) then this model will not hold true [7].

3.2.3 *Population Balance Model (PBM)*

Population (or number) balance equations applicable to chemical engineering were initially developed for the study of crystallization by Hulbert and Katz [11] and Randolph and Larson [12]. They were then applied to other processes, specifically grinding,

agglomeration, flotation, and liquid-liquid extraction processes [13]. They are thus a well established approach for describing systems involving one phase dispersed in another. This methodology was subsequently used by Crundwell and Bryson [14] and Sepulveda and Herbst [13] to model continuous leach reactors. The population balance is a balance over the number of particles in the system, relying on the conservation of particles. By using the simple conservation balance across a steady-state, continuous reactor, which is described as:

IN + GENERATED = OUT + ACCUMULATED,

the following equation is derived [13]:

$$\boxed{\frac{1}{V}\frac{\partial}{\partial t}(V\psi)} + \boxed{\sum\frac{\partial}{\partial \zeta_i}(v_j\psi)} + \boxed{(\overline{D}-\overline{B})} = \boxed{\frac{1}{V}(Q_{in}\psi_{in} - Q_{out}\psi_{out})} \qquad 1$$

accumulation within the reactor | generated within the reactor | death and birth of particles | inlet stream - outlet stream

where

V = volume of reactor stage

t = time

ψ = population density function

ζ = particular value of a property

Q = flowrate

v_j = rate of change of a specific property

$\overline{B}\ \overline{D}$ = birth/death rate functions to account for breakage, coalescence and agglomeration

Further simplification of this equation is possible with the following assumptions [13]:

- The continuous vessel is operating at steady state, so that the first term is zero;
- Two properties of interest can be defined, such as the initial particle size and size of unreacted core d_c;
- The PSD does not alter because of breakage or attrition, hence D=B=0;
- There is no real change in the volumetric flowrate through the reactor. Thus $Q_{in} = Q_{out} = Q$; and
- The vessel is a CSTR, i.e. well-mixed then $\psi_{out} = \psi$ and $C_{out} = C_B$.

This allows equation 1 to simplify to:

$$\frac{\partial}{\partial d_c}(v\psi)=\frac{1}{\tau}(\psi_{in}-\psi) \qquad 2$$

3.2.4 *Doubly Integrated Micromodel (DIM)*

This model treats the entire multistage reactor series as one unit [8]. It is similar to the Segregated Flow Model, but Dixon lists the difference as being the fact that the SFM refers to the concept of fluid micro-mixing and not the suspended solids. For the DIM, if each particle behaves like a tiny batch reactor then the total conversion will equate the sum of the conversion within each particle, yielding the following double integral:

$$1-X_B=\int_0^{L_{\max}}\int_0^{\tau(L)}[1-X_B(L,t)]E(t)dt\times f(l)dL \qquad 3$$

where

X_B = fraction of reacted solids

L = particle size

$E(t)$ = residence time distribution

$f(l)$ = particle size mass-weighted distribution function

Dixon solves this equation by using Gaussian Quadrature.

3.2.5 *Multiple Convolution Integral (MCI)*

The MCI is an extension of the DIM [9] that is able to incorporate different leaching rates, mean residence times and residence time distributions for the various stages in a multi-stage leaching system. So the particle size distribution for tank N+1 is calculated from the exiting PSD from tank N. This method can be solved using Gaussian Quadrature.

The equation for the conversion is [15]:

$$1-X_{BN}=\int_0^{\xi_{\max}}f_N(\xi)d\xi \qquad 4$$

Hence for 4 tanks in series equation 4 becomes [15]:

$$1-X_{B4}=\int_0^{\infty}\xi^3\left[\int_0^{\infty}\int_0^{\infty}\int_0^{\infty}\left(\xi+\sum_{i=1}^{4}\kappa_i\theta_i\right)^{-3}f_0\left(\xi+\sum_{i=1}^{4}\kappa_i\theta_i\right)\prod_{i=1}^{4}e^{-\theta_i}d\theta_1\ldots d\theta_4\right]d\xi \quad (5)$$

where the following dimensions are defined:

$$\xi=\frac{D}{D^*}$$

$$\theta=\frac{t}{\bar{t}}$$

$$\kappa=\frac{\bar{t}}{\tau^*}$$

$$\tau^*=\frac{\rho_B D^*}{2bk_s C_A}$$

And where

$f_N(\xi)$ = normalized particle size distribution of particles leaving the first tank

X_{BN} = fraction reacted in tank N

$\bar{t}$ = mean residence time per tank

D^* = normalizing particle size

D = original particle size

k_s = rate constant

b = stoichiometric coefficient of solid B

C_A = concentration of A

ρ_B = density of B

3.2.6 Segregation Applied to Continuous Bioleach Reactors

Kotsiopoulos et al [10] derive three models (firstly incorporating age distribution, then size distribution then both relationships) to represent bioleaching reactor performance. The average rate of reaction is described as:

$$\overline{r_n^R}=\int_0^{\infty}\int_0^{\infty}r_n'(\theta,l_{0,n})\frac{M_n^P(\theta,l_{0,n})}{V_n^R}\phi_{MS}\,f_{0,n}(l_{0,n})I(\theta)d\theta dl_0$$

where

$\overline{r_n^R}$ = average reactor bioleaching rate

$r_n'(\theta,l_{0,n})$ = particle leaching rate

$M_n^P(\theta, l_{0,n})$ = mass of a single particle

ϕ_{MS} = fraction of pure mineral sulphide in the ore

$f_{0,n}(l_{0,n})$ = normal distribution representing probability of particles in a size range

$I(\theta)$ = internal age distribution of particles

3.2.7 Model Comparisons

Dixon describes the limitations of the Segregated Flow Model (or as he calls it the Doubly Integrated Micromodel) as being the fact that one rate constant is defined for a cascade of tanks, hence the model cannot handle changes in reactor stage size, leaching rate, solution conditions, temperature or slurry flowrate [9]. This can be avoided by calculating the model for each tank individually, but in some cases (where the leaching rate is not a unique function of particle size) this is not sufficient.

Dixon ascribes the limitations of the PBM to the cumbersomeness and complicated methodology as well as the use of population-weighted particle size distributions (accurate for crystallization but not for leaching, where coarse particles dominate the unleached fraction). Also the PBM is only limited to ideal reactors, while the MCI can be applied to non-ideal reactors where the RTD function is known [9].

Crundwell compares the SFM and the PBM and shows that the two models give different results; with the SFM predicting a larger conversion than the PBM. This difference is attributed to the fact the SFM assumes a constant reactant concentration across a train of reactors, when using one residence time density to describe the model (which is the aim of the SFM). The solution to this is to apply the SFM separately across each tank. He suggests that the most appropriate model for continuous leaching reactors is thus the PBM [7].

Kotsiopoulos et al [10] use inlet particle size and residence time as model inputs to develop a model for a bioleach system. Their model specifically states that the incorporation of both the particle size distribution as well as the age distribution functions is required to give an accurate bioleach model superior to the normal PBM.

3.3 Mass Balance Equations

To complete the continuous leaching model, the formulation of mass balances is required to account for the input and output of material in each leaching stage. The overall reaction process in the secondary leach autoclaves occurs in 3 stages:

- Gaseous reactant is injected into the slurry contained in the reactor;
- The gaseous reactant dissolves into the aqueous phase; and
- The dissolved gas reacts with the solid mineral surface.

The general conservation of mass equation for a continuous steady state process is:

IN + GENERATED = OUT + ACCUMULATED **6**

In addition to this equation, two other equations are required to account for the transport of oxygen from the gaseous phase to the aqueous phase as well as the relationship between oxygen concentration and total reactor pressure.

3.3.1 Calculating the Concentration of Oxygen in Water

Henry's law allows us to convert between pressure and concentration of oxygen according to the following equation [16]:

$$k_H = \frac{c_{aq}}{p_{O_2}} \quad \textbf{7}$$

where

k_H = Henry's constant

c_{aq} = aqueous concentration of oxygen

p_{O_2} = partial pressure of oxygen

k_H is dependant on temperature, and the following relationship between the molal concentration of oxygen in water (c_{aq}), the molal concentration of ionic species in water ($(c_{aq})_I$), temperature and the partial pressure of oxygen can be used to calculate k_H (Tromans [17,18]):

$$c_{aq} = p_{O_2} \exp\left(\frac{0.046T^2 + 203.4T \ln(\frac{T}{298}) - (299.4 + 0.092T)(T - 298) - 20591}{8.3144T} \right) \quad \textbf{8}$$

$$\left(c_{aq}\right)_I = c_{aq}\phi$$

$$\phi = \left\{\frac{1}{1+\kappa(C_I)^y}\right\}^n$$

where

c_{aq} = aqueous concentration of oxygen in water

$\left(c_{aq}\right)_I$ = aqueous concentration of oxygen in an ionic solution

C_I = molal concentration of ionic species

and (at 298K and 1atm), for nickel or copper sulphate solutions:

κ = 2.23207

y = 1.115617

n = 0.222794

And for sulphuric acid solutions:

κ = 2.01628

y = 1.253475

n = 0.168954

In the case of multiple ionic species (as we have), the total effective factor ϕ is calculated as follows [17,18]:

$$\phi_{effective} = \phi_1 \times \left(\phi_2 \times \phi_3 \times \ldots \phi_i\right)^{0.8}$$

Where $\phi_1 < \phi_2 < \ldots < \phi_i$

3.3.2 Calculating the Oxygen Mass Transfer Coefficient

The oxygen mass transfer coefficient (denoted $k_L a$) defines the rate of oxygen transfer from gaseous to aqueous. Fick's first law [19] describes the flux of molecular diffusion as follows:

$$J = -D\left(\frac{dC}{dx}\right)$$

where

D = the diffusivity coefficient,

$\frac{dC}{dx}$ = the rate of change of concentration across a boundary

This can be written as [20]:

$$J \cong \frac{D}{\delta}(C_G - C_L)$$

The overall mass transfer coefficient K is defined as:

$K = \frac{D}{\delta}$, where $\frac{1}{K} = \frac{1}{k_L} + \frac{1}{Ek_G}$

where

k_L = liquid side mass transfer coefficient

k_G = gas side mass transfer coefficient

E = angular coefficient of the saturation curve [20]

But $k_L << Ek_G$ and so the equation simplifies to:

$$J \cong k_L(C_G - C_L)$$

Multiplying both sides by the interfacial area/unit volume "*a*", the molar flow is obtained:

$$N_A = k_L a(C_A{}^S - C_A{}^B)$$

Thus the required $k_L a$ can be calculated by using the gas consumed in the system. However this is not always of practical use as the gas consumption is not known. Instead, an empirical methodology, calculated by van't Riet and described by Pieterse [21] for determining the system $k_L a$, which is based on the gas input and power input (i.e. the absorbed agitator power) is more useful:

$$k_L a = \kappa\left(\frac{P_g}{V_L}\right)^{\alpha} v_G{}^{\beta} \quad 9$$

where

κ = constant

P_g = gassed power input or absorbed agitator power under gassed conditions

V_L = volume

v_G = superficial gas flow

α, β = system parameters

For aerated systems two types of power are defined, viz. the ungassed power draw and the gassed power draw, depending on whether gas is being sparged into the reactor or not. The type of agitator employed in each compartment thus needs to be checked to ascertain if the specific power requirement (under gassed and ungassed conditions) is lower than the installed motor power. The power number (a dimensionless number used to characterise agitator blades) is defined in terms of ungassed power [22] by the following equation:

$$N_p = \frac{P_o}{\rho N^3 D^5} \qquad 10$$

where

N = agitator speed

D = agitator blade diameter

P_o = ungassed power draw

ρ = fluid density

Therefore some relationship is needed between ungassed power and gassed power. For certain types of agitators this ratio is provided by the equipment supplier, in other cases the Michel-Muller equation [23] can be used for correlation:

$$P_g = 0.72\left(\frac{P_o^{\,2} N D^3}{Q^{0.56}}\right)^{0.45} \qquad 11$$

where

P_g = gassed power draw

Q = gas flowrate

3.3.3 Particle Size Distribution

Apart from the above equations, and because we are dealing with particle leaching, an approximation for the particle size distribution (PSD) is required. The actual PSD of the

solids in the reactor is measured (using a Malvern particle size analyser or sieve analysis) and reported as a % undersize per size increment. The information is plotted on a graph and various correlations fitted to the data to allow the derivation of an equation that approximates the data. Meier, et al [24] present the commonly used models for particle size distributions as per Table 2:

Table 2 – Commonly used Particle Size Distributions

Name	Equation	Parameters
Power law distribution or GGS (Gates, Gaudin, Schumann)	$Q_3 = \left(\frac{x}{x_{\max}}\right)^m$	x_{max}, m
RRSB distribution (Rosin-Rammler-Sperling-Bennet)	$Q_3(x) = 1 - \exp\left(-\left(\frac{x}{x'}\right)^n\right)$	x', n
Logarithmic normal distribution	$q_3(x) = \frac{1}{x\sigma\sqrt{2\Pi}} \exp\left\{-\frac{1}{2}\left[\frac{\ln\left(\frac{x}{x_{50.3}}\right)}{\sigma}\right]^2\right\}$	σ, $x_{50.3}$
Power law combined with attenuation function	$Q_3 = \frac{1}{2}\left(1 + \tanh\left(\frac{x - x^*}{x^*}\right)\right)\left(\frac{x}{x_{\max}}\right)^m$	x*, x_{max}, m
Truncated log normal distribution	$Q_3(x) = \frac{1}{\sqrt{2\Pi}} \int_{-\infty}^{u} \exp\left(\frac{-t^2}{2}\right) dt$ with $u = \frac{1}{\sigma}\left(\ln\frac{x}{x_{\max} - x} - \ln\frac{x_{50.3}}{x_{\max} - x_{50.3}}\right)$	σ, $x_{50.3}$, x_{max}

where

Q_3 = cumulative PSD

q_3 = density PSD

x = particle size

x' = RRSB parameter

x^* = GGS parameter

x_{max} = GGS parameter

$x_{50.3}$ = median diameter of log normal distribution

σ = standard deviation

3.4 Case Studies

A few specific case studies are summarized below, showing the various approaches used to develop leaching models that may provide assistance in the development of the secondary leach model.

Mao and Peters [25] report on the oxygen pressure leaching of chalcocite (Cu_2S), discovering that the leach exhibits the same 2-stage leach characteristics that occur when chalcocite is dissolved in acidic ferric sulphate. The first stage is the leaching of 100% of the chalcocite to covellite (CuS), possibly via an intermediate digenite ($Cu_{1.8}S$) species, followed by the partial conversion of covellite to elemental sulphur. The first stage (which accounts for ~50% of the total copper extraction) follows a shrinking core behaviour, with the first 20% of the copper extraction pore diffusion controlled, followed by a change to a chemical reaction controlled regime. The pore diffusion controlled phase is possibly attributed to the initial rapid reaction of chalcocite to a covellite layer on the surface of the particle, which takes slightly longer to start reacting. For the second stage leaching, the particles break into a new size distribution (according to SEM of the chalcocite particles during various stages of the leaching) and so the absence of a reaction model makes it difficult to extract rate constant data from the resulting leaching curves. This observation is relevant to the leach tests presented in this study, as the major reactant is a copper mineral: the possibility of particle breakage thus needs to be considered, as well as the possibility of two leach stages being evident.

A new mathematical model was developed for silica-containing zinc ores by Safari et al [5], which incorporates the effect of a thick gelatinous layer around the reacting core that affects the rate of reaction. A shrinking core, shrinking particle model was developed as

it is postulated that a persistent layer of gelatinous silica coats the reacting particles. This was considered of interest for the secondary leach model because in some copper mineral reactions, the formation of elemental sulphur occurs that either coats the reactant particles or forms separate sulphur balls (specifically in high acid conditions).

Velardo et al [26] state that the SCM does not accurately describe the dissolution of solid particles, as the "polydispersity of the solid particle is ignored". In this paper three adjustable parameters are defined, related to the surface topology of the particles and used to account for the depth of surface imperfections, surface heterogeneity and the steepness of the surface imperfections. This seems to be an unnecessary complication of the model: each particle will react individually and thus exhibit a range of surface characteristics. Without accurately measuring these three qualities, the improvement of accuracy in the leaching model is not apparent.

4 LEACH MODEL DEVELOPMENT

Although logic dictates that solution of the model starts with feed data determination, then batch data analysis to obtain kinetic information, followed by the mathematical leach model development that links everything together, the actual approach taken in the development of the model was to first determine the leach model that would be used (PBM or DIM, etc), and from that model work in reverse to ascertain the input data required. Finally the mathematical methodology required to solve the leach model was selected. The steps used to develop the leaching model for the secondary leach application, and the reasoning behind the approach, are shown in Figure 8.

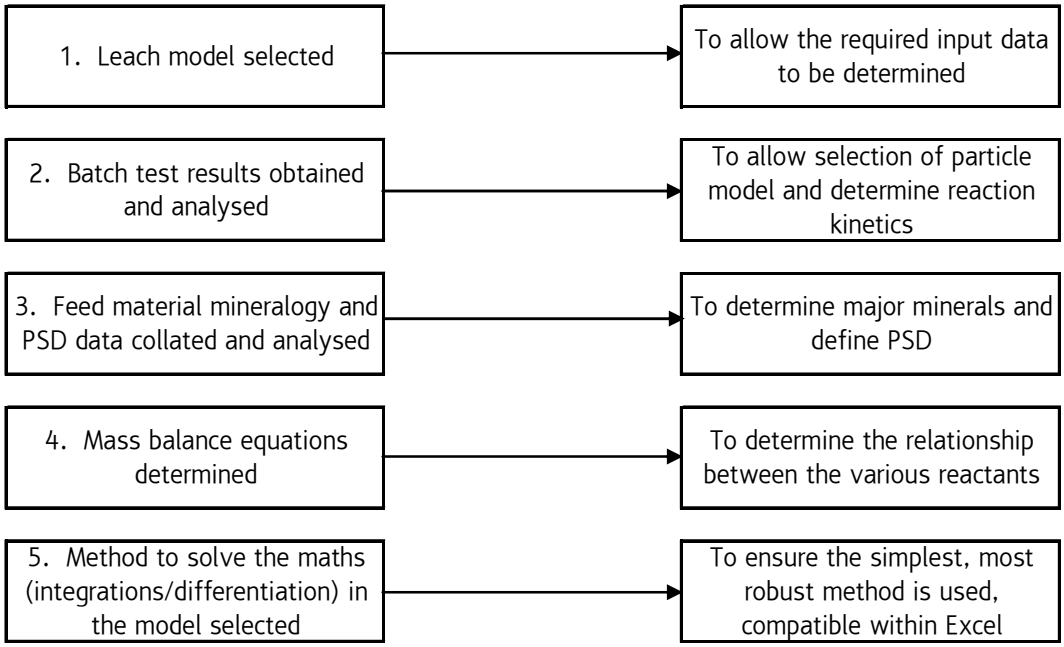

Figure 8 – Summary of Model Development Methodology

Each step is discussed further below.

4.1 Leach Model Selection

Based on the comparison of the various mathematical leach models discussed in Section 3.2, the population balance approach was selected for the secondary leach model development because it seemed to be a simple approach that showed a good correlation to actual plant data, as Crundwell and Bryson [14] showed when they prepared a population balance model and use it to compare actual data from the zinc pressure

reactor at Cominco's plant at Trail, British Columbia (BC). The predictions fit the measured data closely as shown Table 3:

Table 3 – Cumulative Conversions in Each Compartment for the Trail BC Zinc Plant [14]

	Compartment			
	1	2	3	4
Calculated (%)	88.12	95.76	97.86	98.67
Actual (%)	88.7	96.5	97.9	98.4

It is also particularly useful for investigating the effect of atypical particle size distributions on a leach system, which is one of the areas of investigation for this thesis.

4.2 Population Balance Derivation

The derivation of the population balance is best depicted pictorially, with the hatched section of Figure 9 showing a particular size class of material being leached and the arrows depicting flow of particles into or out of the size class, either by flow of slurry through the reactor leach stage or as a result of leaching causing larger particles to enter a specific size class or particles in a specific size class to exit into a smaller size class as they shrink:

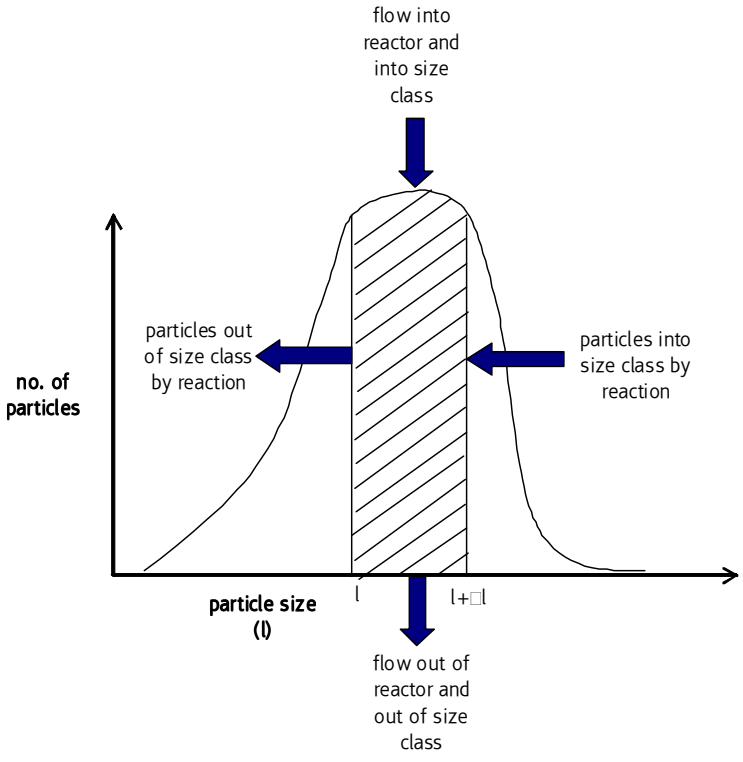

Figure 9 – Graphical Depiction of Particle Population Balance

The number of particles of a particular size class in the reactor at steady state is:

no. of particles into reactor and size class by flow	+	no. of particles into size class by reaction	=	no. of particles out of reactor and size class by flow	+	no. of particles out of size class by reaction

$$n_i(l)\Delta l Q + n_o(l+\Delta l)GV = n_o(l)\Delta l Q + n_o(l)GV \qquad 12$$

where

$n_i(l)$ = number of particles entering reactor per unit volume

$n_o(l)$ = number of particles exiting reactor per unit volume

G = linear shrinkage rate of particles

Q = flowrate of slurry through reactor

V = volume of reactor stage

In this equation the rate of reaction is described with "G", a variable accounting for the linear rate of shrinkage of the particle. So by rearranging Equation 12:

$$\tau G \frac{\left(n_o(l+\Delta l) - n_o(l)\right)}{\Delta l} = n_o(l) - n_i(l)$$

And taking the limits as Δl approaches zero results in the following differential equation:

$$\tau G \frac{dn_o(l)}{dl} = n_o(l) - n_i(l) \qquad 13$$

The solution to this equation will allow us to calculate the number of particles exiting the reactor. The number of particles entering the reactor can be established from the particle size distribution, and the assumption that the particles are spherical. On examination it is apparent that this equation is not a variable separable equation (i.e. it cannot be written in the form $g(y)dy - f(x)dx = 0$) and hence it requires some manipulation in order to obtain a solution. First write the equation in the following form:

$$M(x,y)dx + N(x,y)dy = 0$$

and ascertain whether the equation is exact, by checking $\frac{\partial M}{\partial y} = \frac{\partial N}{\partial x}$, as this is a sufficient test to prove that $M(x,y)dx + N(x,y)dy$ is a total, or exact differential [27]. In this case:

$$[n_o(l) - n_i(l)]dl - \pi G dn_o(l) = 0,$$

where $x = l$ and $y = n_o(l)$

results in $\frac{\partial M}{\partial y} = 1$, and $\frac{\partial N}{\partial x} = 0$

Thus the equation is not exact. The next step is to determine whether the equation can be made exact by multiplying it by a suitable function (referred to as an integrating factor).

Assume $F(x,y)$ is the integrating factor, the differential equation thus becomes [27]:

$$F(x,y)M(x,y)dx + F(x,y)N(x,y)dy = 0$$

Or in simpler annotation:

$$FM + FN = 0$$

Applying the exactness conditions from above [27]

$$\frac{\partial}{\partial y}FM = \frac{\partial}{\partial x}FN$$

To simplify this we assume that the integrating factor F is only a function of one variable (say x).

$$F\frac{\partial M}{\partial y} = \frac{dF}{dx}N + F\frac{\partial N}{\partial x}$$

Re-ordering

$$\frac{1}{F}\frac{dF}{dx} = \frac{1}{N}\left(\frac{\partial M}{\partial y} - \frac{\partial N}{\partial x}\right)$$

And substituting in

$$\frac{1}{F}\frac{dF}{dl} = \frac{1}{-\tau G}(1-0)$$

$$\int \frac{1}{F} dF = -\int \frac{1}{\tau G} dl$$

With the result that

$F = e^{\frac{-l}{\tau G}}$, so re-arranging equation 13 and multiplying it by this integrating factor we obtain

$$\frac{e^{\frac{-l}{\tau G}} dn_o(l)}{dl} - \frac{e^{\frac{-l}{\tau G}} n_o(l)}{\tau G} = \frac{-e^{\frac{-l}{\tau G}} n_i(l)}{\tau G} \qquad \textbf{14}$$

But

$$\frac{d(e^{\frac{-l}{\tau G}} n_o(l))}{dl} = \frac{e^{\frac{-l}{\tau G}} dn_o(l)}{dl} - \frac{e^{\frac{-l}{\tau G}} n_o(l)}{\tau G} \qquad \textbf{15}$$

Thus substituting 15 into 14,

$$\int \frac{d(e^{\frac{-l}{\tau G}} n_o(l))}{dl} dl = \int -e^{\frac{-l}{\tau G}} \frac{n_i(l)}{\tau G} dl$$

Resulting in:

$$n_o(l) = e^{\frac{l}{\tau G}} \int -e^{\frac{-l}{\tau G}} \frac{n_i(l)}{\tau G} dl \qquad \textbf{16}$$

Before solving this integral, the following point requires further investigation: the number of particles of size l, referred to as $n_o(l)$, exiting the leach stage are not solely formed from one size class, but form when several larger size classes leach and diminish in size until they are size "l", as Figure 10 shows:

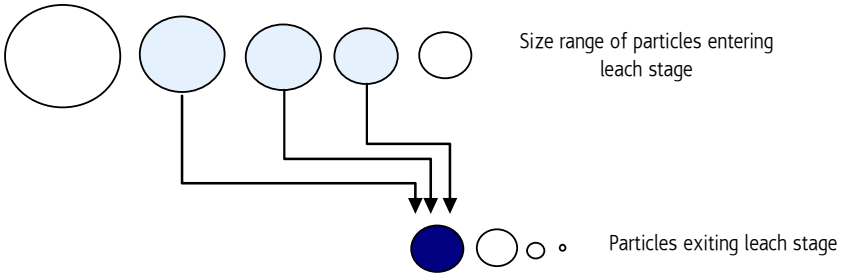

Figure 10 – Example of the Leaching of Particles into a Particular Size Class

In the case where l = 20micron, $n_o(20micron)$ is formed by a number of inlet size class particles - viz. $n_i(25micron)$, $n_i(24micron)$, $n_i(23micron)$, etc - leaching down to 20micron. Therefore the term $n_i(l)$, that forms part of the integral of equation 16, represents a number density function of inlet particles. To represent this more accurately we alter $n_i(l)$ to $n_i(l^*)$ to differentiate between an actual point value and a distribution.

$$n_o(l) = e^{\frac{l}{\pi G}} \int - e^{\frac{-l}{\pi G}} \frac{n_i(l^*)}{\pi G} dl \qquad 17$$

Kumar et al [28] state that the continuous number density function $n(t,x)$ can be approximated using the Dirac delta function as follows:

$$n(t,x) \approx \sum_{i=1}^{I} N_i \delta(x - x_i)$$

where

N_i = number of particles of size class i
$\delta(x - x_i)$ = Dirac delta function

The Dirac delta function is also referred to as the unit impulse function [29], and specifically describes a discontinuous pulse, or is used to model a tall input spike function [30]. Sepulveda and Herbst [13] also utilise it in their derivation of a population balance.

We define:

$$n_i(l^*) \approx \sum_{l=1a}^{l_i} n_i(l_a)\delta(l_a - l)$$ where l_a is a specific particle size class.

Equation 17 transforms to:

$$n_o(l_i) = e^{\frac{l_i}{\pi G}} \int_{l_a}^{l_i} -e^{\frac{-l}{\pi G}} \frac{n_i(l_a)}{\pi G} \delta(l_a - l) dl \qquad \textbf{18}$$

This enables the calculation of the number of particles of size class l_i exiting the reactor/stage as a result of the particles of size l_a entering the reactor.

The Dirac function has the following relevant property [31]:

$$\int_a^b f(x)\delta(x - x_0)dx = \frac{1}{2} f(a) \text{ for } x_0 = a$$
$$= \frac{1}{2} f(b) \text{ for } x_0 = b$$
$$= f(x_0) \text{ for } a < x_0 < b$$

In our case $f(x) = -e^{\frac{-l}{\pi G}} \frac{n_i(l_a)}{\pi G}$ with the limits a = l_a and b = l_i

So the solution to the integral is:

$$n_o(l_i) = \frac{-n_i(l_a)}{\pi G} e^{\frac{(la-l)}{\pi G}} \text{ for } l_a < l < l_i$$
$$n_o(l_i) = \frac{-n_i(l_a)}{2\pi G} e^{\frac{(la-l)}{\pi G}} \text{ for } l = l_a \text{ or } l = l_i \qquad \textbf{19}$$

And hence we have derived an equation quantifying the number of particles of a particular size class exiting a leach stage. Using the following two relationships:

$$m_{out}(l) = \frac{n_o(l) V \rho \pi l^3}{6}$$

$m_{out}(l)$ = mass of particles exiting leach stage in size class l

and

$$n_i(l) = \frac{m_{in,total} Y 6}{V \pi l^3}$$

where

$m_{in,total}$ = total mass of particles entering leach stage

Y = fraction of particles of size l entering leach stage

The mass of particles exiting each leach stage is calculated as follows:

$$m_{out}(l) = \int_{l_{\max}}^{l} \frac{-m_{in}}{\pi G} e^{\frac{(l-l_a)}{\pi G}} \left(\frac{l}{l_a} \right)^3 Y_a dl_a \qquad 20$$

Here Y_a (the fraction of particles entering the reactor in size class l_a) can be obtained from the RRSB [24, 32] approximation or from cubic spline interpolation.

4.3 Linear Shrinkage Rate per Particle

The determination of G, the linear shrinkage rate of the leached particle mentioned in Section 4.2, is discussed further. Often rate constants for chemical reactions are written in terms of moles of material reacting per time, but the PBM requires the linear rate of reaction to be calculated, and its derivation is thus shown. The simplified reaction of a solid reacting with a solid or gaseous reactant can be written as [4]:

$$aA + bB + \ldots \rightarrow products$$

Where A is the aqueous reactant and B represents the solid reactant. To simplify the analysis, the rate equation for this reaction is approximated as:

$$rate = k_s \left[C_A{}^s \right]^n$$

where

k_s = rate constant

$C_A{}^s$ = concentration of A at surface of solid B

n = order of reaction.

Consider 1 particle of B being leached in a bulk concentration of A, as represented in Figure 11, and described by the shrinking particle model [4].

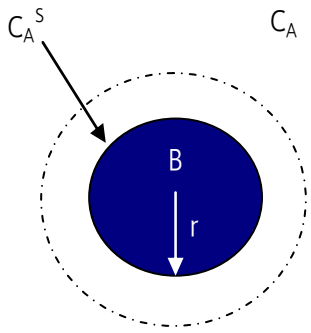

Figure 11 – Particle of B Leaching in Concentration of A

Assuming that the reaction is nth order with respect to the concentration of A, as per Section 4.4.1, then the rate of A consumed per particle per time is [4]:

$$R_A = k_s (C_A^s)^n \pi l^2 \qquad 21$$

Where k_s is the rate constant for the reaction and $l = 2r$.

The rate of disappearance of B is equivalent to the change in number of moles of B over time [4]:

$$R_B = \frac{dN_B}{dt} \qquad 22$$

And assuming spherical particles, the volume per particle is

$V_p = \frac{\pi}{6} l^3$. Using the molar density of B, $N_B = \rho_B \frac{\pi}{6} l^3$ and taking the derivative of this equation:

$$dN_B = d(\rho_B \frac{\pi}{6} l^3)$$

$$dN_B = \rho_B \frac{\pi}{6} \pi d(l^3)$$

$$dN_B = \rho_B \frac{\pi}{6} 3l^2 dl$$

$$\frac{dN_B}{dl} = \frac{\pi}{2} l^2 \rho_B$$

But from the chain rule [33] it is clear that:

$$\frac{dN_B}{dt} = \frac{dN_B}{dl}\frac{dl}{dt}$$
$$\frac{dN_B}{dt} = \frac{\pi}{2} l^2 \rho_B \frac{dl}{dt}$$
$$R_B = \frac{\pi}{2} l^2 \rho_B \frac{dl}{dt}$$

From the stoichiometry:

$$R_B = \frac{b}{a} R_A$$

Therefore:

$$\frac{b}{a} R_A = \frac{\pi}{2} l^2 \rho_B \frac{dl}{dt}$$
$$\frac{b}{a} k_s (C_A^s)^n \pi l^2 = \frac{\pi}{2} l^2 \rho_B \frac{dl}{dt}$$

Re-arranging to obtain:

$$\frac{dl}{dt} = \frac{2bk_s (C_a{}^s)^n}{a\rho_B}$$

Which is defined as the linear shrinkage rate, G:

$$G = \frac{2bk_s (C_a{}^s)^n}{a\rho_B} \qquad 23$$

This equation requires that the rate constant and reaction order are known. These 2 parameters are determined from the batch test data, as detailed in Section 4.4.

4.4 Batch Tests

The results of two sets of batch tests were used for analysis. The first set was conducted at Sherritt Gordon in Canada during 2006 [34] as part of a pilot campaign to develop a new flowsheet for the BMR with slightly different chemistry and the second set was completed at Anglo Research Centre (ARC) in Germiston during 2009 specifically to assist with trying to determine why Anglo Platinum was obtaining such poor leach

efficiencies in the plant. During the tests at ARC special care was taken to control the feed solution and maintain high L:S ratios in the various leach tests to ensure that:

- the acid concentration did not vary substantially across the leach period; and
- the tests were not mass transfer limited.

Both sets of results (shown in Appendix 1 and Appendix 2) were analysed so that the required kinetic data (viz. activation energy, Arrhenius constant and reaction order) could be derived and the leaching mechanism approximated.

A set of five batch reactions were completed for each batch set at different temperatures (but constant pressure) and at different pressures (but constant temperatures), to yield the set of rate constant data listed in Table 4.

Table 4 – Summary of Rate Constants obtained from Batch Tests at Various Temperatures and Pressures

		Constant Temperature T1	Constant Pressure P1
Pressure	P1	k_s(T1,P1)	
	P2	k_s(T1,P2)	
	P3	k_s(T1,P3)	
Temperature	T2		k_s(T2,P1)
	T3		k_s(T3,P1)

4.4.1 *Calculating the Rate Constant*

As copper comprises >50% of the feed material, the copper extractions, measured during the batch tests, were used to evaluate the batch data. The first stage of batch data analysis involved selecting a specific particle model and using the batch results to ascertain if the model was appropriate. The simplest model or shrinking core/shrinking particle model was selected, and various rate-limiting cases analysed (viz. chemical reaction limiting, aqueous phase diffusion limiting and product layer diffusion limiting) to determine if any of them offered a suitable approximation to the secondary leach [35].

Assuming that the concentration of A at the surface of particle B is constant, or the chemical reaction is rate limiting, we obtain the following equation [4]:

$$1-(1-X)^{\frac{1}{3}} = \frac{2bk_s(C_A{}^S)^n t}{aL\rho_B} \qquad 24$$

If the above assumption is valid then this equation is of the straight line form where $y = mx$, and so by plotting 1-(1-X)$^{1/3}$ versus t for all cases (constant temperature and

constant pressure) we obtain a straight line and can calculate the rate constant from the slope [4]. These graphs for the Sherritt pilot data and the Anglo Research data are shown in Figure 12 and Figure 13.

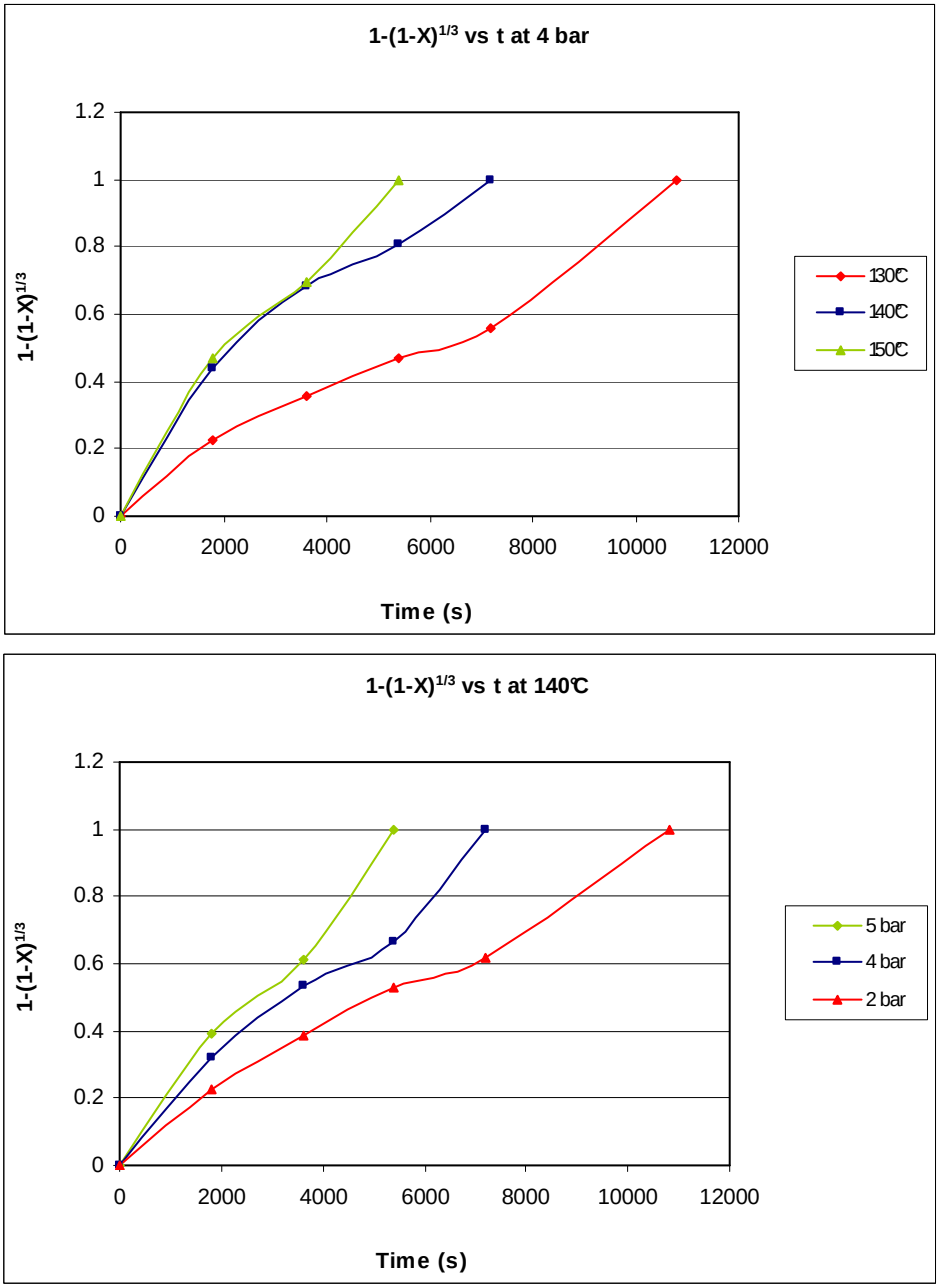

Figure 12 – Sherritt Batch Data at Constant Pressure (4 bar) and Temperature (140°C)

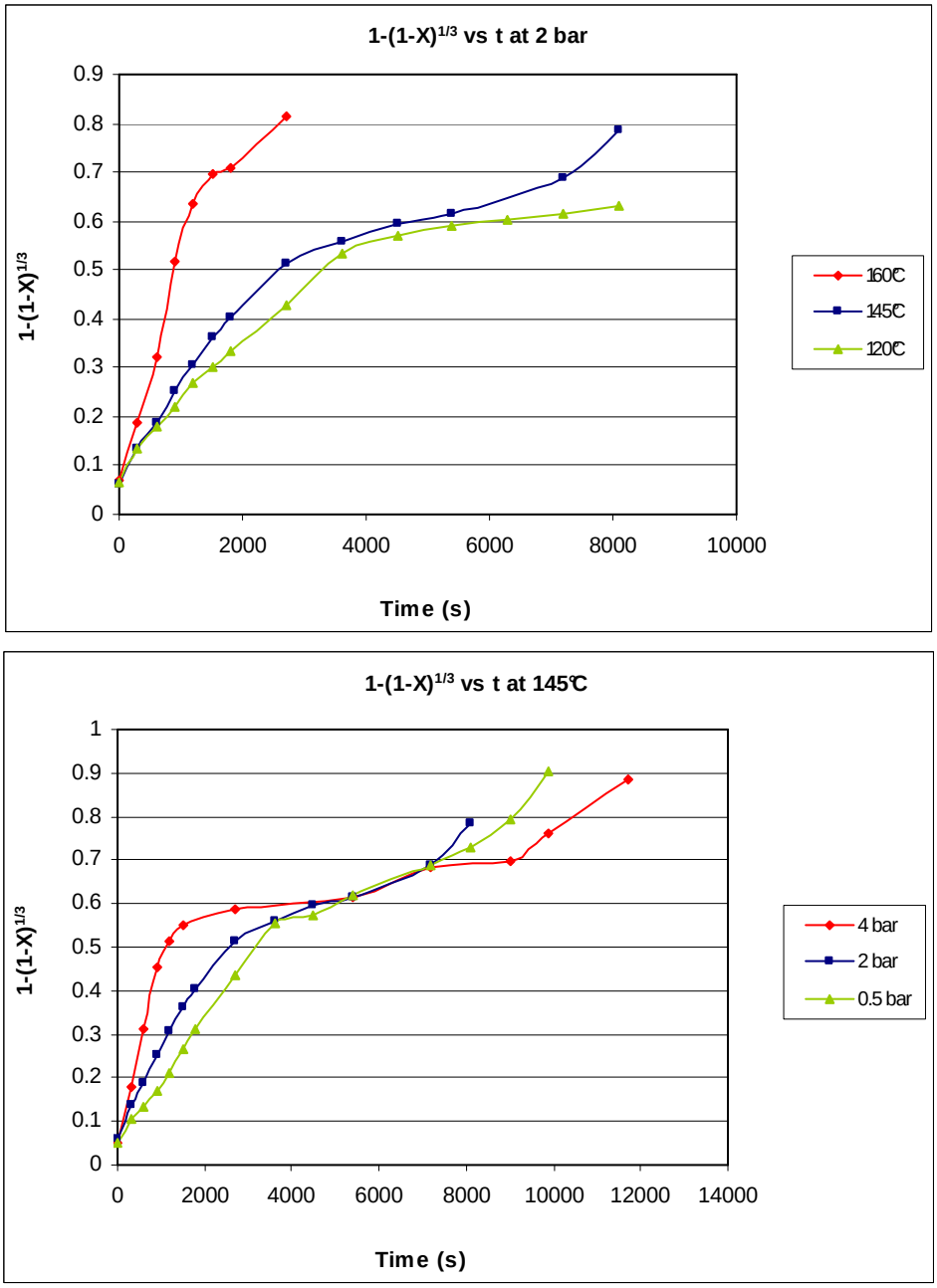

Figure 13 – Anglo Batch Data at Constant Pressure (2 bar) and Temperature (145°C)

In the case of aqueous phase diffusion being rate limiting, then a plot of $1-(1-X)^{(1-n)/3}$ - where n is typically -0.5 - versus time would yield a straight line [4]. These plots for the two sets of batch data are shown in Figure 14 and Figure 15.

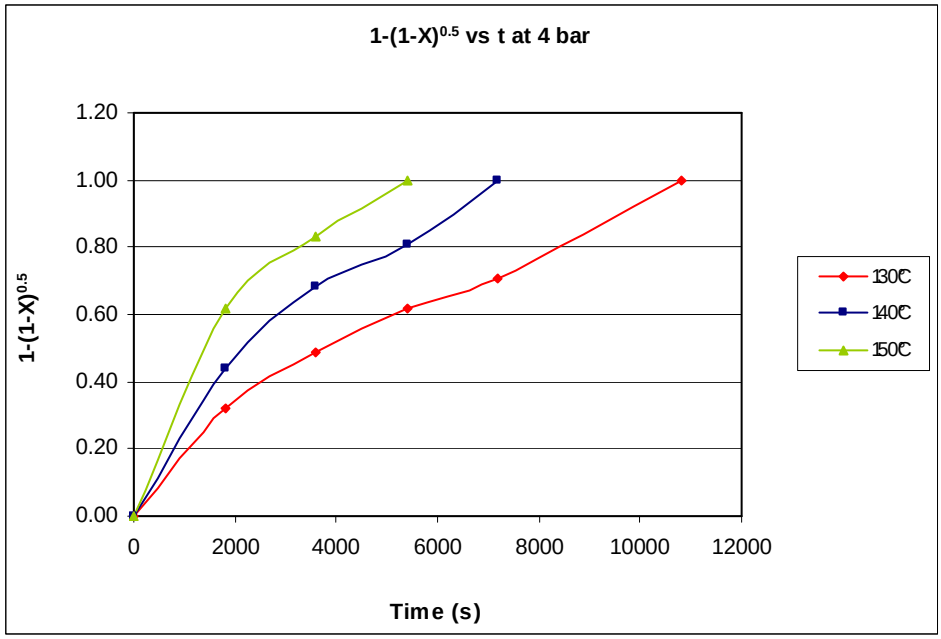

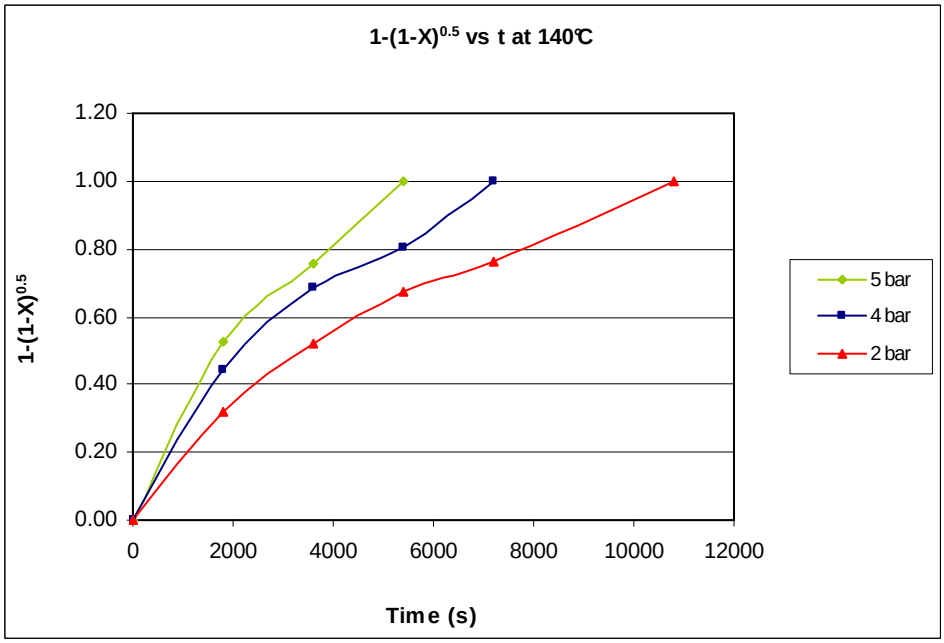

Figure 14 – Sherritt Batch Data at Constant Pressure (4 bar) and Temperature (140°C)

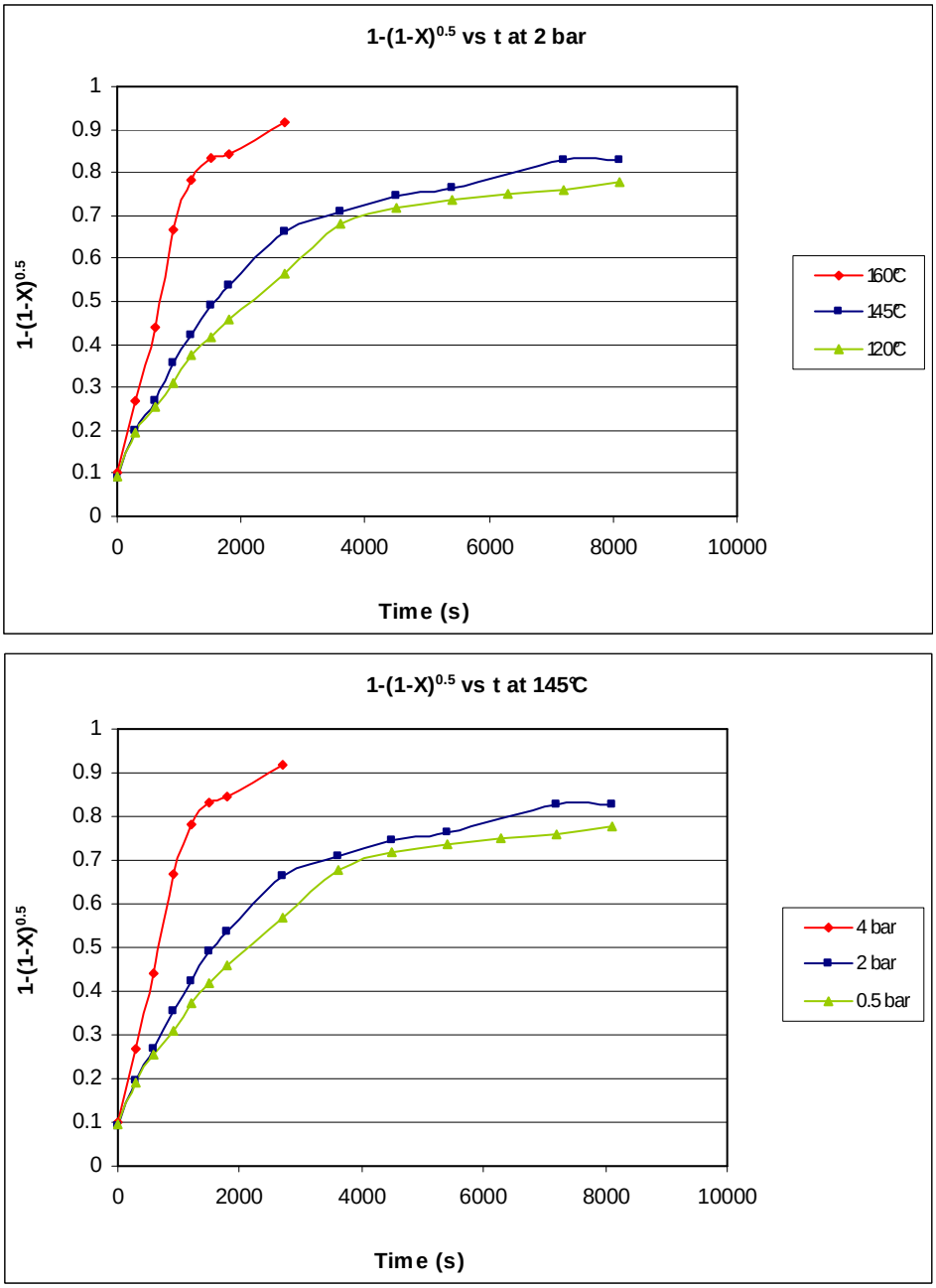

Figure 15 – Anglo Batch Data at Constant Pressure (2 bar) and Temperature (145°C)

If the product layer diffusion is the rate limiting step then a plot of $1-3(1-X)^{2/3}+2(1-X)$ versus time would yield a straight line [4]. These graphs are shown in Figure 16 and Figure 17.

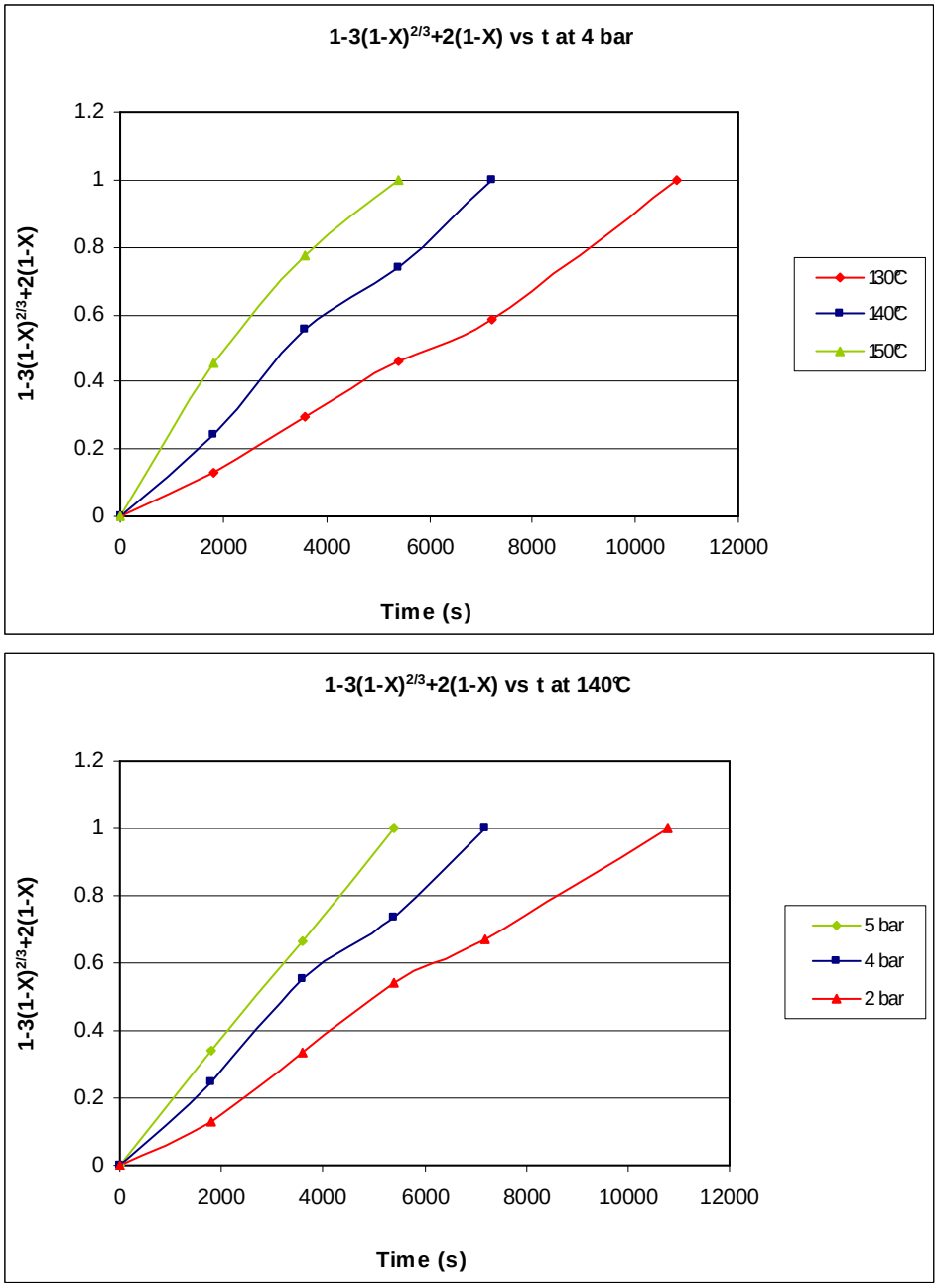

Figure 16 – Sherritt Batch Data at Constant Pressure (4 bar) and Temperature (140°C)

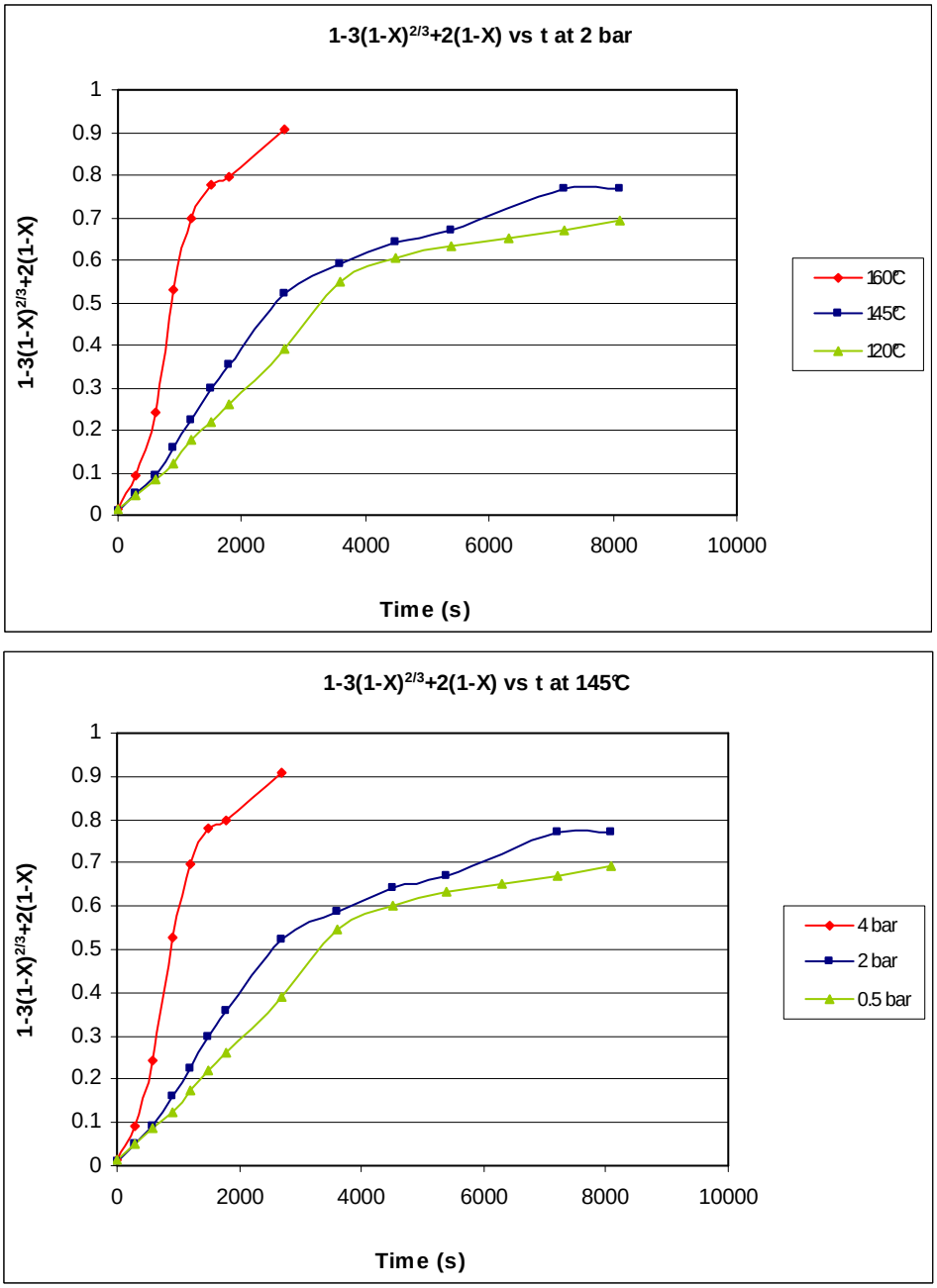

Figure 17 – Anglo Batch Data at Constant Pressure (2 bar) and Temperature (145°C)

None of the graphs shown above represent continuous straight lines; the Sherritt graphs for all three cases are quite similar and can possibly be approximated to a straight line, allowing for some error in the batch data. For this reason the chemical reaction controlled approximation is the most reasonable and simplest approximation for the Sherritt tests.

The Anglo Research data appears to comprise two intersecting straight-line sections with two separate slopes, as shown in Figure 18, indicative of two separate reaction regimes,

possibly indicating two types of reaction (as the inflection in the line occurs at around 90% conversion) or indicating experimental error. The observation that the lines possibly represent two separate reaction regimes is investigated further below.

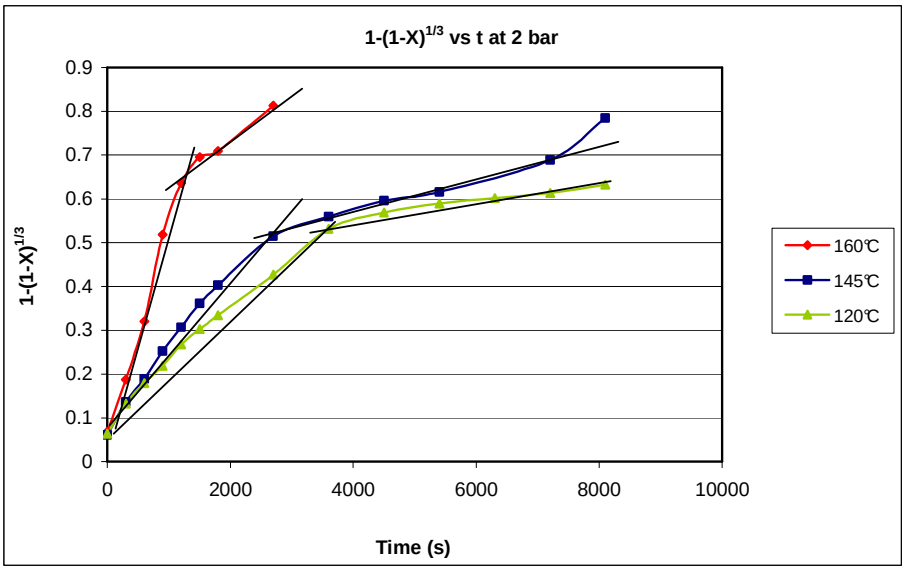

Figure 18 – Anglo Research Batch Data at Constant Pressure (2 bar)

The first possibility is that the leach reaction is divided into two separate rate controlling stages (for example initially chemical reaction rate controlled followed by diffusion controlled if some sort of layer were forming around the leach particles). A possible explanation would be the formation of melted elemental sulphur on the leach particles. However, as the chemical reaction controlled plots are of two intersecting straight lines, the possibility that both stages are chemical rate controlled is high, just occurring at different rates. The second possibility is that two separate chemical reactions are occurring over time. The historical mineralogy shows the major copper minerals evident in the secondary leach feed material to be copper sulphide species (covellite and digenite). Based on the stoichiometric amounts of copper, nickel, iron and sulphur, the copper can be approximated to Cu_2S. This is a simplification made to ascertain if approximations from literature regarding Cu_2S are valid.

Crundwell [36] prescribes a leaching model which describes the leaching of copper sulphide as occurring in two stages:

- A leach step from Cu_2S to CuS and $CuSO_4$ and then
- Further leaching of the CuS to $CuSO_4$.

His depiction of this is shown in Figure 19, as a shrinking core within a shrinking particle:

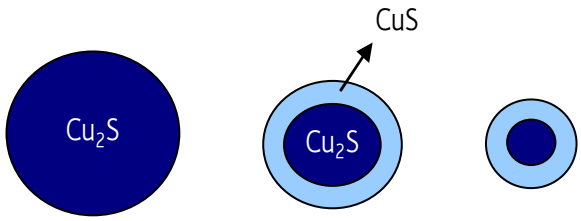

Figure 19 – Shrinking Core of Cu_2S within a Shrinking Particle of CuS

Solving this with a population balance model approach, and realizing that the particles are characterized by two sizes (viz. the diameter of the shrinking core of Cu_2S and the diameter of the shrinking particle of CuS), an equation with two linear rates of particle shrinkage (or G values) is obtained. Thus two rate constants are required (one for the reaction of Cu_2S and one for the reaction of CuS). As the leaching of CuS is known to be slower than Cu_2S, and the apparent occurrence of two reaction regimes in the Anglo Research batch data, this does not seem to be a bad approximation. The challenge, however, is to try and extract the kinetic parameters for each of the leach regimes from the batch data.

Further reading regarding this showed that Homma et al [37] develop a heterogeneous model representing a two step reaction: the formation of a solid intermediate on the core of unreacted solid followed by the consumption of the solid intermediate. This model, described as a shrinking particle within an unreacted shrinking core also allows for relationships between the two characteristic particle sizes (diameter of shrinking particle and diameter of shrinking core) to be developed. The methodology allows for the development of a complicated equation relating the two relevant radii - that of the reactant and that of the total particle – which is inclusive of the intermediate product material.

In trying to apply the above rationale to our data, the following was completed: From the batch data, the two separate leach regimes observed are attributed to two types of leaching with the first stage representing the simultaneous leaching of Cu_2S and CuS, and the second stage representing the leaching of CuS – the slower reacting mineral - only. As the reaction of Cu_2S occurs faster than CuS, we assume that a layer of CuS forms on the shrinking core of Cu_2S almost immediately. This first stage of leaching measured in the batch test is depicted in Figure 20.

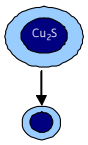

Figure 20 – Possible Approximation for Anglo Batch Data First Leach Stage

Stage 1 would be followed by Stage 2 (that commences where the inflection point is noticed in the Anglo batch data) where the chalcocite has reacted completely and the covellite leaches further, as shown in Figure 21.

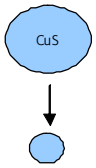

Figure 21 – Possible Approximation for Anglo Batch Data Second Leach Stage

Selecting the shrinking core/shrinking particle model and replotting each set of constant pressure data from Anglo Research as two separate straight lines the following graph (Figure 22) is produced, showing that each graph can be broken into two lines, which seems to agree with the two stage model.

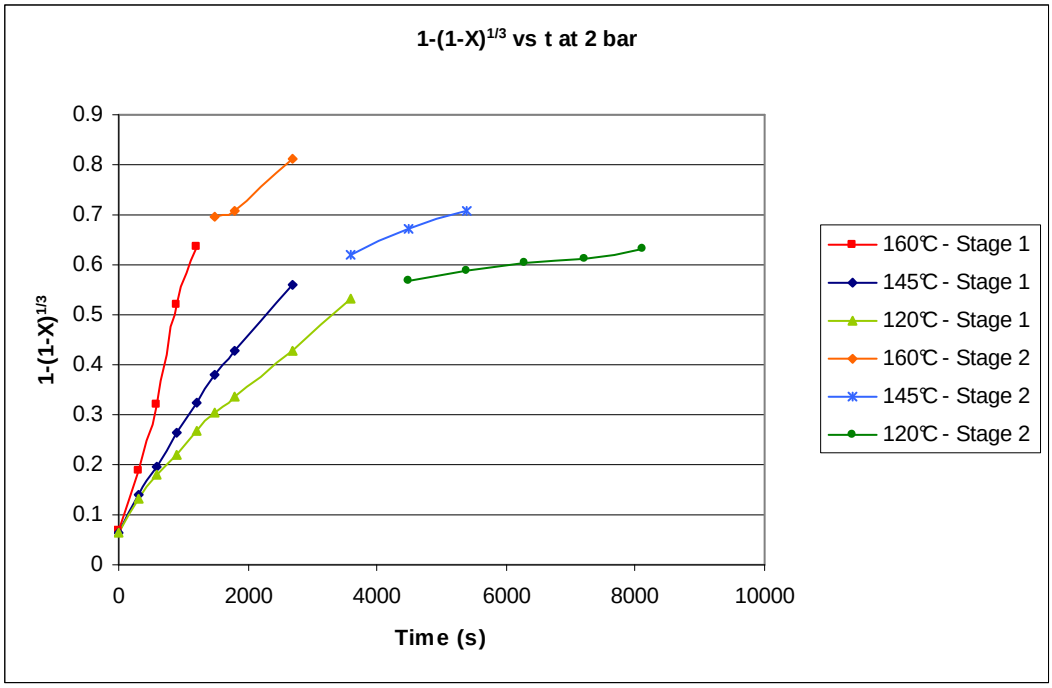

Figure 22 – Replot of Batch Results at Constant Pressure

However the plot for constant temperature yields the following graph:

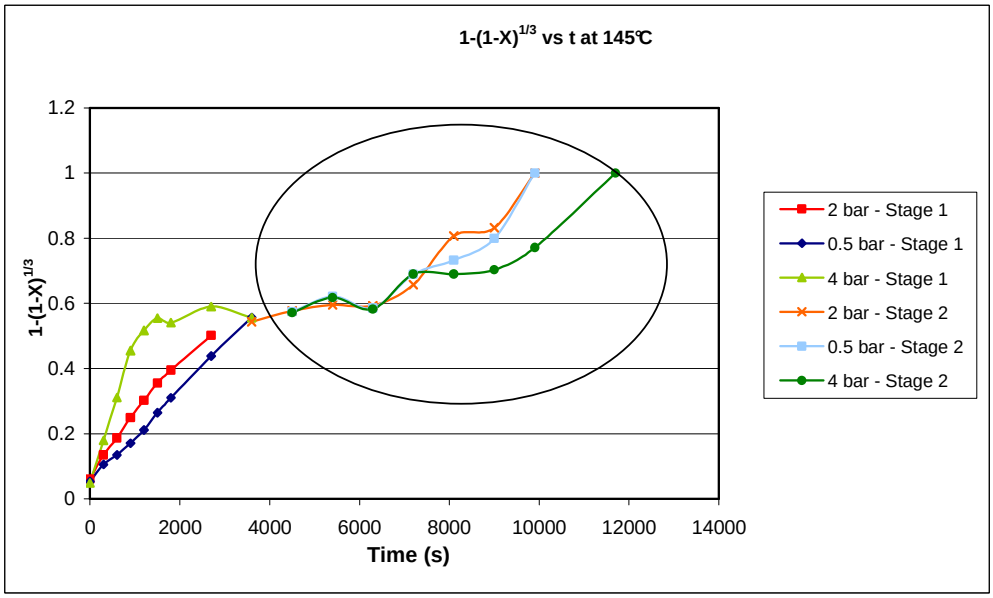

Figure 23 – Replot of Anglo Batch Results at Constant Temperature

The area circled in Figure 23 highlights the second stage of leaching postulated, and shows no great differentiation between the various pressures, even though the reaction is assumed to be covellite reacting with oxygen to form copper sulphate. Further

analysis (to determine the activation energy, Arrhenius constant and reaction order) of this data proved problematic and unstable and yielded a kinetic equation that was close to zero order with respect to the oxygen concentration in the reactor. As Mao and Peters [25] reported (refer to the literature review section), their second stage leaching of chalcocite occurred with particle breakage that resulted in a new PSD. The determination of a meaningful model for this second stage was thus not possible.

Because the Sherritt data showed no noticeable inflection point, and as the second stage noticed in the Anglo Research results occurred at around 90% overall copper conversion, the tail end of these graphs (past 90% conversion) was ignored to simplify the model. The conclusions from the batch data results are as follows:

- The reaction can be approximated by using a shrinking core or shrinking particle model (even though this is not the correct model to use for a porous particle it fits the data better. The model is then considered semi-empirical for this application but as the aim of the modeling is to investigate PSD and external mass transfer which are unaffected by the presence or absence of a core, this assumption is acceptable) ; and
- The reaction is assumed to be the leaching of chalcocite and covellite, occurring simultaneously in one stage. The reactions selected for the copper reaction in the secondary leach autoclaves are thus:

$$Cu_2S + \frac{1}{2}O_2 + H_2SO_4 \rightarrow CuS + CuSO_4 + H_2O$$

Which is then followed by the reaction of covellite to copper sulphate:

$$CuS + 2O_2 \rightarrow CuSO_4$$

To simplify the model further, and because we are assuming that these two reactions are occurring concurrently, they can be combined together to obtain one reaction:

$$\frac{5}{2}O_2 + Cu_2S + H_2SO_4 \rightarrow 2CuSO_4 + H_2O$$

which is the equation used for copper reacting in the model.

Thus by using the shrinking core/shrinking particle approximation the rate constant for each batch case can be determined.

4.4.2 *Calculating the Activation Energy, Reaction Order and Arrhenius Constant*

Using the methodology listed below, and the rate constants as a function of pressure and temperature derived in Section 4.4.1, the activation energy, Arrhenius constant and reaction order are determined for both sets of data. Activation energy is an intrinsic quality that should be determined for each element or molecule but due to difficulties associated with trying to account for all mineral species, the below approximation is deemed suitable.

From the Arrhenius equation it is assumed that the relationship between T and k_s is [4]:

$$k_s = A\exp\left(\frac{-E_a}{RT}\right) \qquad 25$$

where

A = Arrhenius constant

E_a = activation energy

R = universal gas constant

T = temperature

Multiplying both the LHS and the RHS by $\left[C_A{}^s\right]^n$ and taking the natural logarithm of both sides, equation 25 is transformed into a form of the straight line equation $y = mx + c$:

$$\ln\left(\left[C_A{}^s\right]^n k_s\right) = n\ln\left[C_A{}^s\right] + \ln A - \frac{E_a}{RT}$$

Thus at constant temperature but varying oxygen partial pressure, a plot of $\ln\left(\left[C_A{}^s\right]^n k_s\right)$ versus $\ln\left[C_A{}^s\right]$ should yield a straight line with slope equivalent to n and y-intercept equivalent to $\ln A - \frac{E_a}{RT}$, whereas at constant oxygen partial pressure but varying

temperature a plot of $\ln\left(\left[C_A{}^s\right]^n k_s\right)$ versus $\frac{1}{T}$ should yield a straight line graph with slope equivalent to $\frac{-E_a}{R}$ and y-intercept equivalent to $n\ln\left[C_A{}^s\right]+\ln A$.

(The Excel excerpt of this, with graphs, for the Anglo Research data, appears in Appendix 3). A comparison between the two batch sets of data is shown below in Table 5. The activation energy value for both sets of batch data (>40 000J/mol) substantiates the assumption that the reaction is chemical rate controlled [4], and the reaction order of 0.51 is the same for both sets of data, so this is used in the model. The Arrhenius constant is 612 for the Anglo Research data and 513 for the Sherritt data. This difference is caused by differences in the feed materials. The Anglo Research value was used in the model, as this data is more recent and the feed material used in the batch tests is a more accurate approximation of the current plant's feedstock.

Table 5 – Comparison of Kinetic Parameters obtained from Batch Data Results

	Sherritt Data	Anglo Research Data
Activation Energy (J/mol)	51 944	45 646
Arrhenius constant	513	612
n (reaction order)	0.51	0.51

4.4.3 Reactions Selected

The reactions selected for the copper leaching in the secondary leach autoclave are the simplified reaction summarising the leaching of chalcocite and covellite to copper sulphate (refer to Section 4.4.1):

$$\frac{5}{2}O_2 + Cu_2S + H_2SO_4 \rightarrow 2CuSO_4 + H_2O$$

and the equation describing the transfer of oxygen from the gaseous phase to the aqueous phase, the rate of which is controlled by a mass-transfer coefficient or $k_L a$:

$$O_{2(g)} \rightarrow O_{2_{(aq)}}$$

4.5 Feed Material

4.5.1 Mineralogy

The mineralogy of the feed to the secondary leach autoclaves varies within a range. The extent of the range and variances needed to be determined. Three separate mineralogical analyses, completed at different periods of time were therefore compared. These mineralogical analyses were then simplified into the major elemental constituents to determine which element was dominant and thus ascertain if the feed mineralogy could be simplified in any manner.

A comparison of some historical mineralogy (reported in 1995 [38], 2001 [2] and 2006 [39]) to the most recent mineralogy (2009 [40]) is summarised in Table 6. The 2006 mineralogy classifies the copper sulphides as 'intermediate copper sulphides'. The mineralogy for 1995 and 2001 is quite similar with digenite and covellite dominating as copper minerals and polydimite and millerite as nickel minerals, but the recent mineralogy (2009) shows far more detail in terms of mineral composition. Only 0.8% of covellite is measured in 2009, compared to 30-35% reported in previous years, and far more minerals are represented (like natrojarosite, idaite, anilite and fletcherite).

There are various reasons for the differences. The 2009 analysis utilizes a bulk modal analysis technique (referred to as MLA – comprising a scanning electron microscope with an energy dispersive x-ray spectrometer), whereas the earlier analyses were conducted using x-ray diffraction (XRD). So where polydimite (Ni_3S_4) was previously identified, the MLA technique calls this phase fletcherite ($(CuNi_2)S_4$) as the beam diameter used cannot resolve the fine precipitated/cemented copper sulphide in the nickel sulphide [41]. The copper-iron sulphides reported in 1995 are recorded as idaite in 2009 and certain phases (like the pentlandite, alumina-rich silicates, oxides an jarosite) that appear in 2009 would not be detectable via XRD [41].

Table 6 – Mineralogical Composition of Feed Material

Mineral (%)	1995[38]	2001[2]	2006[39]	2009[40]
Ni_3S_4	12	12-6		
NiS	5	6-4		
Int Cu-sulphide			62.4	
Cu_9S_5	30	30-35		0.8

Mineral (%)	1995[38]	2001[2]	2006[39]	2009[40]
CuS	35	40-45		50.7
$Cu_3(OH)_4SO_4$	5	0-5		
Cu-Fe sulphides	5			
$NaFe_3(SO_4)_2(OH)_6$				0.7
$CuSO_4.5H_2O$			15.6	
Cu_5FeS_4			7.8	
Cu_5FeS_6				3.4
Cu_7S_5				12.6
$CuNi_2S_4$			13.8	30.5
$(Fe,Ni)_9S_8$				0.7
Fe,Cr-oxide				0.2
Al_2O_3				0.2
$Al_2SiO_5/Al_{4.5}Si_{1.5}O_{9.75}$				0.1

In summary: the mineralogical analysis is not accurate in providing an accurate quantitative analysis of minerals. From a chemical content point of view, however, the comparison between the four separate analyses shows that the proportion of copper, nickel, iron and sulphur present in the secondary leach feed stream is reasonably constant and similar, as shown in Table 7, with the copper ranging from 47-66%, the nickel from 8-12%, the iron from 0.3-5% and the sulphur from 24-31%.

Table 7 – Chemical Composition of Secondary Leach Feed Material

Element (%)	1995[38]	2001[2]	2006[39]	2009[40]
Cu	50	47-55	66.4	55.02
Ni	10	12-8	8.8	11.56
Fe	3	2.5-5.0	0.3	1.41
S	26	24-27	27.5	30.85

For the purposes of this model the following simplifications are therefore made: As the material comprises greater than ~50% copper, and assuming that the nickel occurs as polydimite (because it is the major nickel constituent noted in the 1995 and 2001 data), and that the iron occurs as a simple iron sulphide (not an unreasonable assumption as the

iron is apparent in such small relative quantities), the copper mineralogy can be approximated to Cu_xS. The determination of "x" is shown in Table 8 as being ~2.

Table 8 – Derivation of Stoichiometric amount of Sulphur Associated with Copper

			tph	kmol/hr
Cu		55%	0.88	13.85
Ni		9%	0.1424	2.43
Fe		1%	0.016	0.29
S		26%	0.416	13.00
		Ni/Fe/Cu	S	kmol/hr
Ni_3S_4		2.43	3.23	0.81
FeS		0.29	0.29	0.29
total			3.52	
Cu_xS		13.85	9.48	6.92
		x	1.46	

A ratio of copper to sulphur of 2 was used in the model development and is in agreement with the simplifications postulated in Section 4.4.1.

4.5.2 Particle Size Distribution

The mathematical leach model being developed in this paper requires an equation to approximate the PSD of the material in each leach stage, based on the feed PSD. Actual PSDs of secondary leach feed material were thus compared for two reasons: firstly to obtain a brief view of the variance in particle size that the plant experiences, and secondly to decide whether a particle size model could be used to approximate the data.

The feed material to the BMR plant currently has a d95 of 45 micron [42]. Two separate sets of particle size distributions for the feed material to the secondary leach autoclaves were obtained for comparison, the first set from the Sherritt Pilot Test campaign that was run during 2006 [34] and the second set during a plant trial in 2009 [42]. (Refer to Appendix 4 for the actual data.)

The PSD from the Sherritt 2006 pilot plant campaign exhibits a d90 of 41micron and a d50 of 16.4micron while the 2009 plant data has a d90 of 61 micron and a d50 of 23 micron. The differences in the PSDs are attributed to the slightly different leach conditions and the different feed material used for the two separate sets of data. Also noticeable is that the Sherritt data exhibits a unimodal, normal type distribution (Figure 24), while the 2009 plant data has a bimodal appearance (Figure 25), with a coarse fraction evident in the range of ~90 micron.

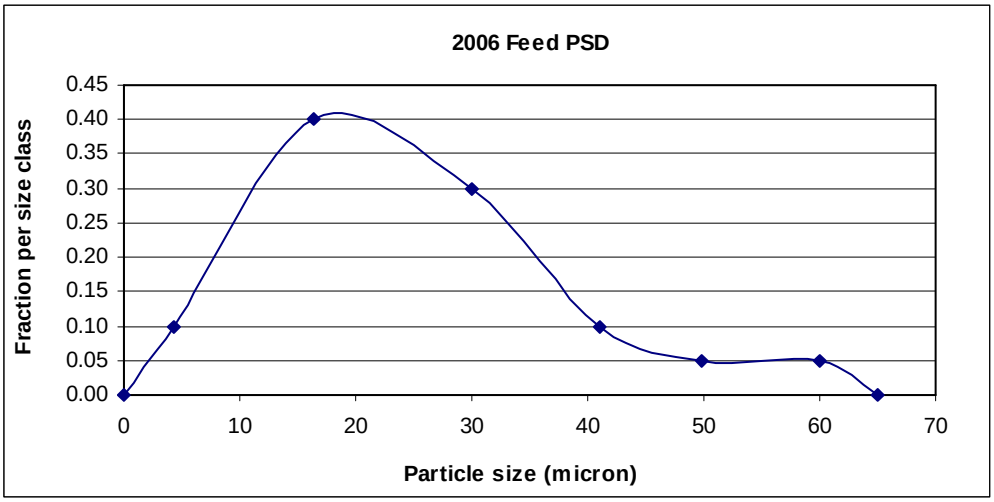

Figure 24 – Sherritt Feed PSD from Pilot Plant Operation

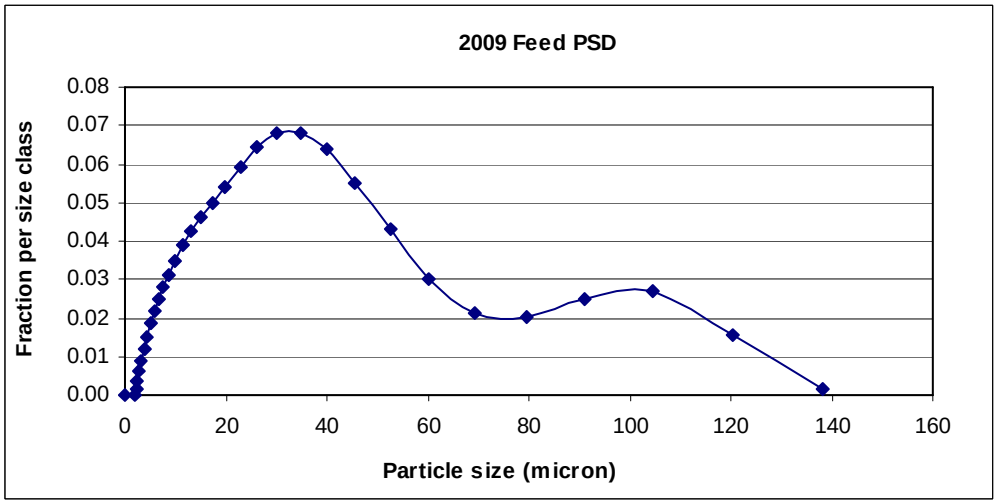

Figure 25 – Feed PSD from 2009 BMR Plant Trial

To account for the changing PSD through the leach in each separate leach stage, a PSD model or approximation is required that can be incorporated into the overall leach model. The Rosin-Rammler-Sperling-Bennet (RRSB) [24, 32] equation, which is commonly used for PSD modeling, was used for this:

$$Y = 1 - \exp\left[-\left(\frac{X}{X'}\right)^{n}\right] \qquad 26$$

where

Y = the cumulative fraction of particle by undersize

X = the particle size

X' = a parameter for size dimension

n = dimensionless exponent

The comparison between the actual plant data and the RRSB fit - for both the 2006 Sherritt data and 2009 plant data - is shown in Figure 26 and Figure 27 below:

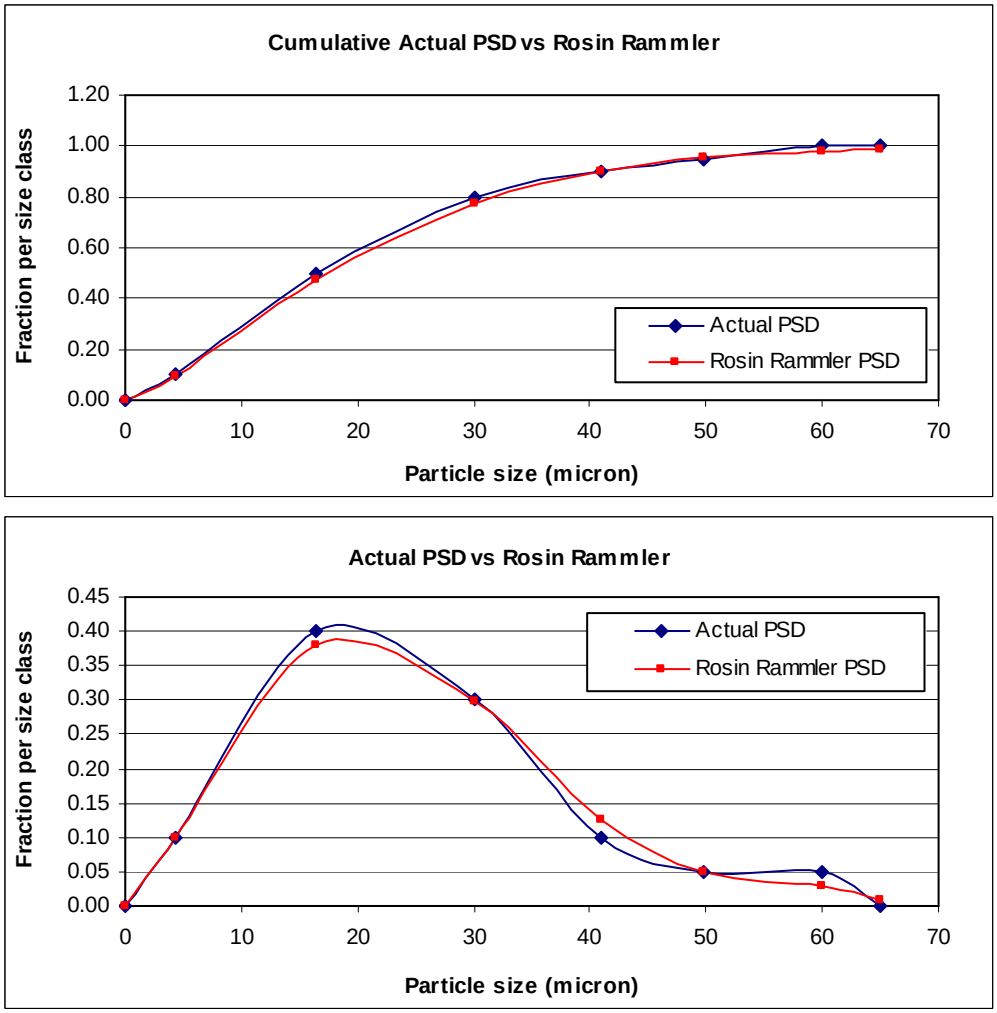

Figure 26 – Actual Size Distribution versus RRSB for 2006 Sherritt Data

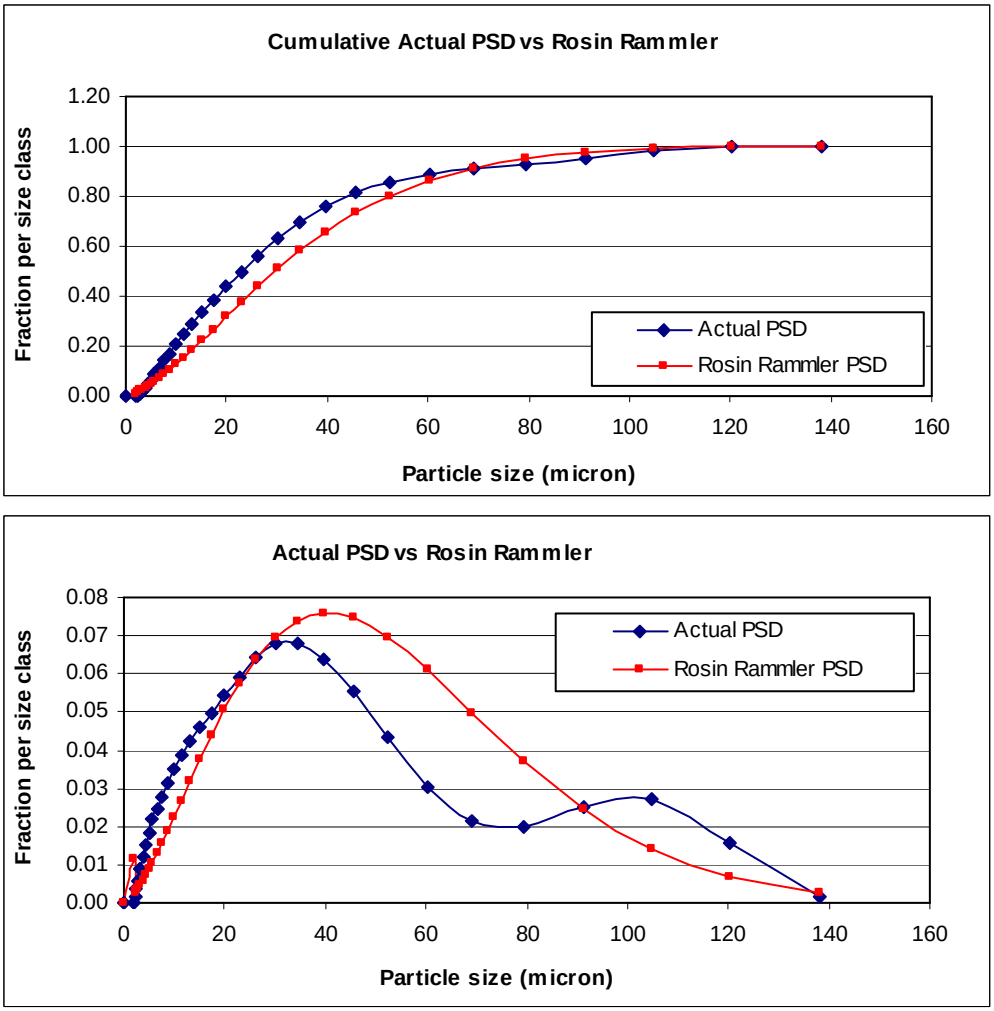

Figure 27 – Actual Size Distribution versus RRSB for 2009 Plant Data

The 2006 data agreement between actual data and the RRSB model appears fair; however the 2009 data - which exhibits the bimodal distribution - is not well represented using a RRSB model as the data is smoothed out to a unimodal distribution. This is clearly shown on the graph depicting the fraction per size class versus the particle size, but is not as clear on the cumulative graph. So the RRSB model was disregarded as suitable for inclusion in the overall leach model and although other particle models are available (as discussed in Section 3.3.3), the method of using cubic spline interpolation to fit particle size class to actual fraction of particles [43] was selected because it allows a simple method for closely fitting actual data and is easy to incorporate into an Excel platform. The cubic spline fit to the 2009 PSD is shown in Figure 28.

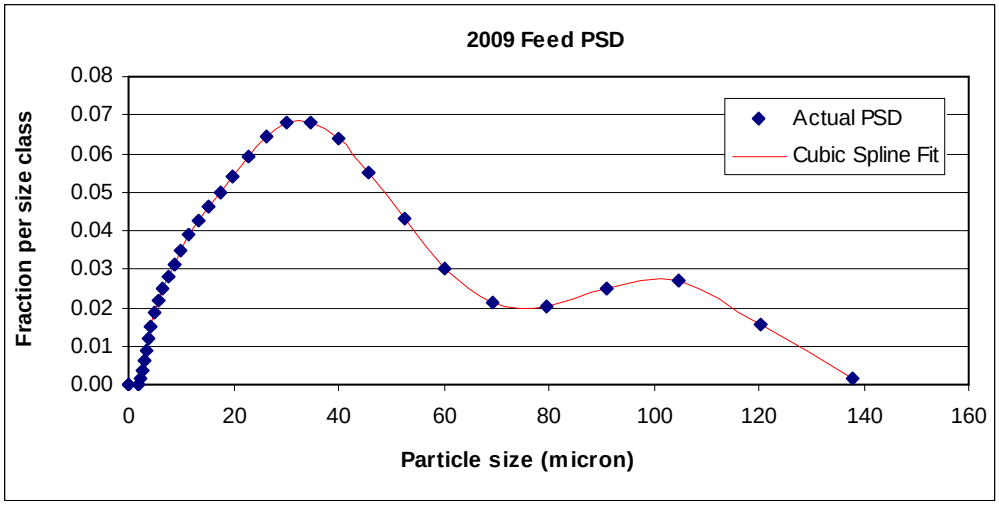

Figure 28 – Cubic Spline fit to Actual Feed Material

The effect on copper recovery of using the RRSB approximation versus fitting actual data using cubic spline interpolation is compared during the model evaluation in Section 5.2.

4.6 Mass Balances

4.6.1 Copper

The copper mass balance was developed using the conservation of mass, Equation 6, and utilising the population balance model to determine the copper conversion over each stage.

4.6.2 Oxygen (Reactant A)

Two mass balances are calculated for the oxygen

- The overall mass balance over oxygen in the slurry system, in the aqueous phase shown in Figure 29; and
- The mass balance of oxygen in the gaseous phase.

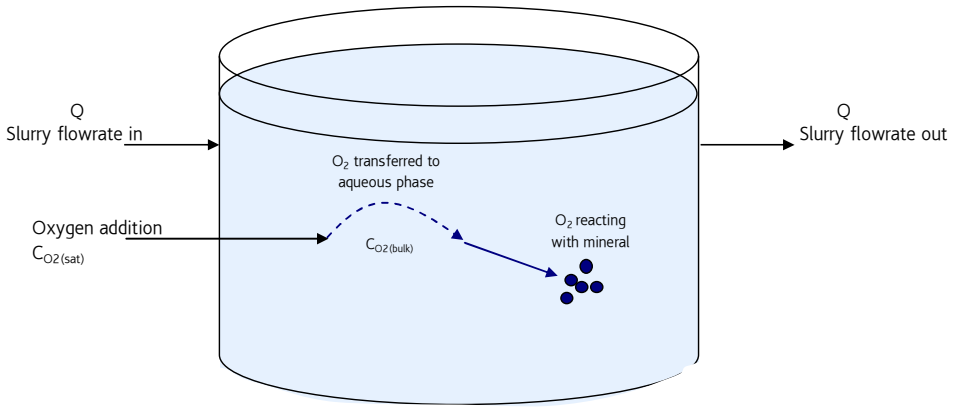

Figure 29 – Representation of Leach Slurry System

The overall mass balance over oxygen (or reactant A) in the slurry system, in simple terms is:

oxygen entering reactor with slurry flow	+	oxygen transferred from gaseous to aqueous phase	=	oxygen reacting with mineral	+	oxygen out of reactor with slurry flow

$$C_A^{\,in}Q + k_L a(C_A^{\,sat} - C_A^{\,bulk})V = \frac{a}{b} m_B X + C_A^{\,out}Q$$

where

$C_A^{\,in}$ = concentration of A entering the leach stage

$C_A^{\,sat}$ = saturated concentration of A

$C_A^{\,bulk}$ = bulk concentration of A

m_B = molar flowrate of B

Re-arranging this equation in terms of the saturated concentration of A:

$$C_A^{\,sat} = \frac{\frac{a}{b} m_B X + QC_A^{\,bulk} + k_L aVC_A^{\,bulk} - QC_A^{\,in}}{k_L aV} \qquad 27$$

The mass balance of oxygen in the gaseous phase:

oxygen injected into the reactor in gaseous phase	=	oxygen leaving reactor in gaseous phase	+	oxygen transferred from gaseous to aqueous phase

$$C_A^{bulk} = C_A^{sat} - \frac{(m_A^{in} - m_A^{out})}{k_L a V} \quad (28)$$

where

m_A = molar flowrate of A

C_A^{sat} is calculated according to the Tromans equations [17,18] listed in Section 3.3.1, which derates the C_A^{sat} obtained in water by a factor of ~0.73 for the ionic leach solution, assuming the following concentrations:

Copper = 40g/l
Nickel = 20g/l
Iron = 5g/l
Sulphuric acid = 10g/l

Additional equations are required for the relationship between the other gaseous components in the gas stream (water and nitrogen):

$$m_T = \frac{m_{N_2}}{\left(1 - \frac{p_w}{P_T} - x_{O_2}\right)} \quad (29)$$

where

m_t = total gas molar flow

m_{N_2} = molar flow of nitrogen

p_w = partial pressure of water

P_T = total system pressure

x_{O_2} = molar fraction of oxygen

and for the relationship between the total molar flow of gaseous particles to the fraction of oxygen:

$$m_{O_2} = m_T x_{O_2} \quad (30)$$

where

m_{O_2} = molar flow of oxygen

4.7 Mathematical Solution of Leach Model

There are two possible mathematical methods of solving the PBM. The first (presented by Bryson and Crundwell and reported in an internal Anglo Platinum report [42]) uses the differential population balance equation (Equation 12), re-arranged as follows:

$$n_0(l) = \frac{n_i(l)Q\Delta l + n_0(l+\Delta l)GV}{Q\Delta l + GV}$$

Then by stepping down through a range of particle sizes, starting with the largest size class, and understanding the boundary condition that $n_0(l+\Delta l)$ is zero for the largest size class, the number of particles of a particular size exiting the reactor can be calculated for each step. This method is referred to as the Step-Through Method (STM) in this paper.

The second method involves solving the final PBM equation (equation 20). This cannot be solved analytically so the equation was then solved using a simple numerical method, viz. Simpson's rule [44]. This method is referred to as the Numerical Simpson's Method (NSM) in this paper.

Both methods were used and the results obtained are compared in Section 5 of this report.

4.8 Excel Implementation of Model

The various mass balance and number balance equations for the copper and oxygen reactions need to be solved iteratively to obtain the conversion of copper in the reactor. The methodology followed is shown in Figure 30.

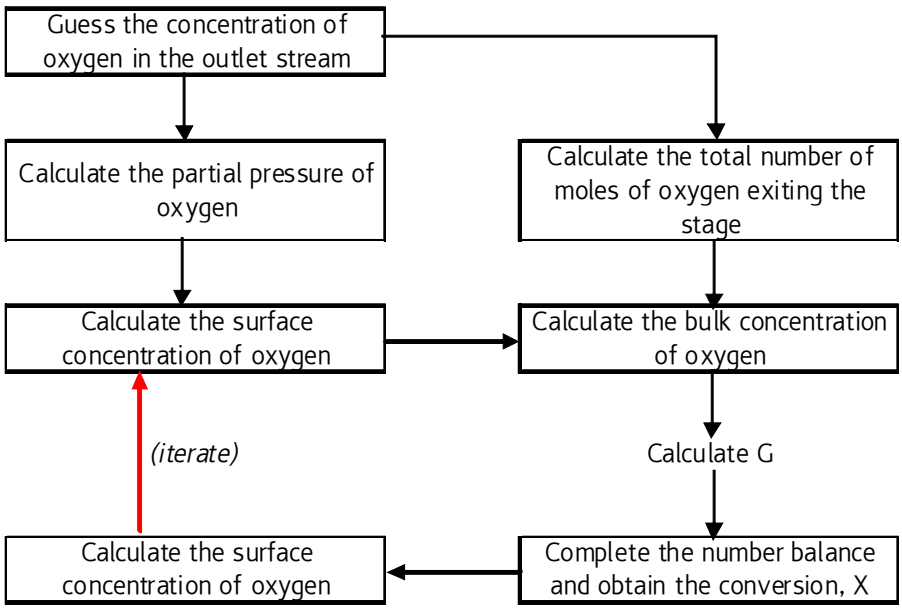

Figure 30 – Calculation Logic for each Leach Stage

Both the Step-Through Method (STM) and the Numerical Simpson's Method (NSM) were set-up in Excel, with the inclusion of Visual Basic code (shown in Appendix 5) to solve the Simpson's Integration in the Numerical Model and the cubic spline interpolation [43] used in both models. The NSM set-up is shown in
Figure 31.

Numerical Method (using Simpson's Rule)

{Press the solve button to calculate the 4 goal-seeks - one for each leach stage - automatically}

Simpson's integral increments 100

	fraction undersize	STAGE 1	l_i		mass particles in	particles out	
	feed		m	ni(l)	tph	tph	
		l_0					
4.84E-05	4.84E-05	l_1	1.91E-06	1.14E+11	0.0001	0.0009	9.22E-11
1.56E-03	1.51E-03	l_2	2.19E-06	2.36E+12	0.0017	0.0014	3.31E-09
5.13E-03	3.56E-03	l_3	2.51E-06	3.67E+12	0.0039	0.0021	8.95E-09
1.11E-02	6.00E-03	l_4	2.88E-06	4.08E+12	0.0066	0.0029	1.73E-08
1.99E-02	8.72E-03	l_5	3.31E-06	3.92E+12	0.0096	0.0038	2.89E-08
3.18E-02	1.20E-02	l_6	3.80E-06	3.55E+12	0.0132	0.0050	4.55E-08
4.71E-02	1.53E-02	l_7	4.37E-06	2.99E+12	0.0168	0.0064	6.66E-08
6.56E-02	1.86E-02	l_8	5.01E-06	2.41E+12	0.0204	0.0079	9.30E-08
8.74E-02	2.17E-02	l_9	5.75E-06	1.86E+12	0.0239	0.0097	1.25E-07
1.12E-01	2.48E-02	l_{10}	6.61E-06	1.40E+12	0.0273	0.0117	1.64E-07
1.40E-01	2.79E-02	l_{11}	7.59E-06	1.04E+12	0.0307	0.0140	2.11E-07
1.71E-01	3.13E-02	l_{12}	8.71E-06	7.73E+11	0.0345	0.0166	2.73E-07
2.06E-01	3.49E-02	l_{13}	1.00E-05	5.70E+11	0.0385	0.0195	3.49E-07
2.45E-01	3.87E-02	l_{14}	1.15E-05	4.18E+11	0.0427	0.0226	4.45E-07
2.87E-01	4.24E-02	l_{15}	1.32E-05	3.02E+11	0.0467	0.0260	5.59E-07
3.33E-01	4.60E-02	l_{16}	1.51E-05	2.16E+11	0.0507	0.0297	6.96E-07
3.83E-01	4.97E-02	l_{17}	1.74E-05	1.55E+11	0.0548	0.0339	8.64E-07
4.37E-01	5.41E-02	l_{18}	2.00E-05	1.11E+11	0.0596	0.0386	1.08E-06
4.96E-01	5.93E-02	l_{19}	2.29E-05	8.04E+10	0.0653	0.0435	1.36E-06
5.61E-01	6.43E-02	l_{20}	2.63E-05	5.77E+10	0.0709	0.0479	1.69E-06
6.29E-01	6.78E-02	l_{21}	3.02E-05	4.02E+10	0.0747	0.0506	2.05E-06
6.97E-01	6.80E-02	l_{22}	3.47E-05	2.66E+10	0.0750	0.0510	2.36E-06
7.61E-01	6.39E-02	l_{23}	3.98E-05	1.65E+10	0.0705	0.0478	2.55E-06
8.16E-01	5.53E-02	l_{24}	4.57E-05	9.45E+09	0.0610	0.0411	2.53E-06
8.59E-01	4.32E-02	l_{25}	5.25E-05	4.88E+09	0.0476	0.0320	2.27E-06
8.89E-01	3.01E-02	l_{26}	6.03E-05	2.25E+09	0.0332	0.0232	1.82E-06
9.10E-01	2.12E-02	l_{27}	6.92E-05	1.05E+09	0.0234	0.0189	1.47E-06
9.31E-01	2.01E-02	l_{28}	7.94E-05	6.55E+08	0.0222	0.0198	1.60E-06
9.56E-01	2.50E-02	l_{29}	9.12E-05	5.38E+08	0.0275	0.0245	2.28E-06
9.83E-01	2.71E-02	l_{30}	1.05E-04	3.86E+08	0.0299	0.0247	2.84E-06
9.98E-01	1.56E-02	l_{31}	1.20E-04	1.47E+08	0.0172	0.0126	1.88E-06
1.00E+00	1.74E-03	l_{32}	1.38E-04	1.08E+07	0.0019		2.41E-07
	1.00			**3.02E+13**	**1.10**	**0.69**	3.19E-05
					stage recovery	37.35%	
					overall recovery	**86.30%**	

SLURRY IN						
CO_2 in	0.02	mol/m³				
GAS IN						
air flowrate	2800	Nm³/hr	125 000	mol/hr		
O_2 conc	0.34	mol O2/mol air				
O_2 flowrate	42 500	mol/hr				
N_2 flowrate	82 500	mol/hr				
AUTOCLAVE						
kla	596.34	/hr				
temperature	143.9	℃	417.05	K		
pressure	1138	kPa(a)				
ks	0.00036					
Q	10.392	m³/hr				
V	19.9615	m³		KO_2	0.000913	(mol/l)/atm
T	6915.283544			pO_2	0.91	kPa
G	6.03E-10	m/s		CO_2bulk	0.01	mol/m³
k	2.64E+05					
H_2O vapour	400.27	kPa				
enriched air	737.73	kPa		1.056155024		
CO_2sat	1.09	mol/m³				
GAS OUT						
nwater	61054.34989	mol/hr				
pO_2	196.87	kPa				
CO_2sat	1.06	mol/m³	H_2O out			
ntotal	173584.2	mol/hr	61 054	mol/hr		
nO_2 out	30029.9	mol/hr		12 470		
CO_2bulk	0.01	mol/m³				
0.04 xO_2 out	0.17	GUESS				
off-gas conc	26.69%	O_2				
utilisation	29.34%	O_2				

Figure 31 – Numerical Method for Solving Leach Model

And the STM in Figure 32:

STEP THROUGH METHOD

STAGE 1

Q	0.00288658	m³/s		10.391678				{Press the solve button to calculate the 4 goal-seeks -					
G	7.57E-10	m/s						one for each leach stage - automatically}					
V	19.9615	m³	k	k									
	K		0.000138038	0.05	0.1						13848.2359		
	h		0.000017812	362.219099	724.438198			35.90%					
					1.10	3.02E+13	1.66E+13	0.71		**SLURRY IN**			
l	l	cumu. Frac	frac	mass in	ni(l)	n0(l)	mass out	cub spline		CO_2 in	0.02	mol/m³	
micron	m												
138.038	0.00013804	1.00E+00	1.74E-03	1.92E-03	1.08E+07	8.36E+06	0.001484055	1.74E-03					
120.226	0.00012023	9.98E-01	1.56E-02	1.72E-02	1.47E+08	1.12E+08	0.013111094	1.56E-02		**GAS IN**			
104.713	0.00010471	9.83E-01	2.71E-02	2.99E-02	3.86E+08	3.09E+08	0.023980982	2.71E-02		air flowrate	2800	Nm³/hr	125 000 mol/hr
91.201	9.1201E-05	9.56E-01	2.50E-02	2.75E-02	5.38E+08	4.67E+08	0.023937124	2.50E-02		O_2 conc	0.34	mol O2/mol air	
79.433	7.9433E-05	9.31E-01	2.01E-02	2.22E-02	6.55E+08	5.92E+08	0.020022601	2.01E-02		O_2 flowrate	42 500	mol/hr	
69.183	6.9183E-05	9.10E-01	2.12E-02	2.34E-02	1.05E+09	8.78E+08	0.019637031	2.12E-02		N_2 flowrate	82 500	mol/hr	
60.256	6.0256E-05	8.89E-01	3.01E-02	3.32E-02	2.25E+09	1.70E+09	0.025065751	3.01E-02		**AUTOCLAVE**			
52.481	5.2481E-05	8.59E-01	4.32E-02	4.76E-02	4.88E+09	3.49E+09	0.034065351	4.32E-02		kla	596.34	/hr	
45.709	4.5709E-05	8.16E-01	5.53E-02	6.10E-02	9.45E+09	6.65E+09	0.042883358	5.53E-02		temperature	143.9	℃	417.05 K
39.811	3.9811E-05	7.61E-01	6.39E-02	7.05E-02	1.65E+10	1.15E+10	0.049196896	6.39E-02		pressure	1138	kPa(a)	
34.674	3.4674E-05	6.97E-01	6.80E-02	7.50E-02	2.66E+10	1.85E+10	0.05208436	6.80E-02		ks	0.00036		
30.2	0.0000302	6.29E-01	6.78E-02	7.47E-02	4.02E+10	2.78E+10	0.051617244	6.78E-02		Q	10.392	m³/hr	
26.303	2.6303E-05	5.61E-01	6.43E-02	7.09E-02	5.77E+10	3.95E+10	0.048582799	6.43E-02		V	19.9615	m³	
22.909	2.2909E-05	4.96E-01	5.93E-02	6.53E-02	8.04E+10	5.43E+10	0.04408118	5.93E-02		T	6915.28354		
19.953	1.9953E-05	4.37E-01	5.41E-02	5.96E-02	1.11E+11	7.31E+10	0.039188423	5.41E-02		G	7.57E-10	m/s	
17.378	1.7378E-05	3.83E-01	4.97E-02	5.48E-02	1.55E+11	9.75E+10	0.034547902	4.97E-02		k			
15.138	1.5138E-05	3.33E-01	4.60E-02	5.07E-02	2.16E+11	1.30E+11	0.030407725	4.60E-02		H_2O vapour	400.27	kPa	
13.183	1.3183E-05	2.87E-01	4.24E-02	4.67E-02	3.02E+11	1.72E+11	0.026615303	4.24E-02		enriched air	737.73	kPa	
11.482	1.1482E-05	2.45E-01	3.87E-02	4.27E-02	4.18E+11	2.26E+11	0.023121503	3.87E-02		CO_2sat	1.06	mol/m³	
10	0.00001	2.06E-01	3.49E-02	3.85E-02	5.70E+11	2.94E+11	0.019861666	3.49E-02		**GAS OUT**			
8.71	0.00000871	1.71E-01	3.13E-02	3.45E-02	7.73E+11	3.79E+11	0.016899694	3.13E-02		nwater	61076.9112	mol/hr	
7.586	7.586E-06	1.40E-01	2.79E-02	3.07E-02	1.04E+12	4.83E+11	0.014244905	2.79E-02		pO_2	197.07	kPa	
6.607	6.607E-06	1.12E-01	2.48E-02	2.73E-02	1.40E+12	6.12E+11	0.01192086	2.48E-02		CO_2sat	1.06	mol/m³	H_2O out
5.754	5.754E-06	8.74E-02	2.17E-02	2.39E-02	1.86E+12	7.67E+11	0.009870267	2.17E-02		ntotal	173648.4	mol/hr	61 077 mol/hr
5.012	5.012E-06	6.56E-02	1.86E-02	2.04E-02	2.41E+12	9.48E+11	0.008054938	1.86E-02		nO_2 out	30071.5	mol/hr	
4.365	4.365E-06	4.71E-02	1.53E-02	1.68E-02	2.99E+12	1.15E+12	0.006437358	1.53E-02		CO_2bulk	0.01	mol/m³	
3.802	3.802E-06	3.18E-02	1.20E-02	1.32E-02	3.55E+12	1.35E+12	0.005019809	1.20E-02	0.00	xO_2 out	0.17	GUESS	
3.311	3.311E-06	1.99E-02	8.72E-03	9.61E-03	3.92E+12	1.55E+12	0.003790393	8.72E-03		off-gas conc	26.71%	O_2	
2.884	2.884E-06	1.11E-02	6.00E-03	6.61E-03	4.08E+12	1.71E+12	0.002777525	6.00E-03		utilisation	29.24%	O_2	
2.512	2.512E-06	5.13E-03	3.56E-03	3.93E-03	3.67E+12	1.83E+12	0.001957413	3.56E-03					
2.188	2.188E-06	1.56E-03	1.51E-03	1.67E-03	2.36E+12	1.86E+12	0.0013127	1.51E-03					
1.905	1.905E-06	4.84E-05	4.84E-05	5.33E-05	1.14E+11	1.39E+12	0.0006494	4.84E-05					
0	0	0.00E+00	0.00E+00	0.00E+00		1.39E+12	0	0.00E+00					

Figure 32 – Step-Through Method for Solving the Leach Model

5 RESULTS

5.1 Model Evaluation

After both models were compiled in Excel, the following steps were completed to evaluate them:

- The copper recovery calculated on the plant in three separate trials was compared to the copper recovery predictions of both the STM and the NSM models;
- The copper recovery obtained when using the RRSB PSD approximation instead of the actual PSD data – specifically for the bimodal PSD noticed in 2009 - was predicted using the NSM;
- The PSD measured in the plant for each leach stage during the 2009 plant trials was compared to the PSD determined by both of the models;
- The effect of different combinations of Rushton (denoted R) and A315 agitators (denoted A) in the autoclave compartments on the copper recovery was compared.

5.2 Comparison with Actual Plant Data

During 1997 a detailed plant trial, investigating the oxygen enrichment of the secondary autoclaves, was completed by Hofirek [1]. This data was used for the initial model set-up and comparison and is referred to as Trial 1. In April 2009 a course on leaching was presented to students on the Graduate Development Program presented by Crundwell and Bryson, culminating in a final report [42]. During the course, several plant runs were completed on the secondary autoclaves, with the process parameters and final copper extraction recorded. Data from two of these trials, taken from the report, is used in this paper and referred to as Trial 2a and Trial 2b. These three sets of data, listed in Table 9, were used to compare the predicted recoveries (from the STM and the NSM) to actual plant recoveries.

Table 9 – Plant Test Trial Parameters

		Trial 1 [1,42]	Trial 2a [42]	Trial 2b [42]
PSD Characteristic		Unimodal	Bimodal	Bimodal
Agitator configuration		R-R-A-A	R-A-A-R	R-A-A-R
Autoclave feed rate				
PLR throughput rate	tph	1.68	1.6	2.09

		Trial 1 [1,42]	Trial 2a [42]	Trial 2b [42]
Slurry feed rate	m^3/hr	10.8	10.1	13.3
PLR composition				
Cu	%	48.5	53.9	41.5
Ni	%	12.9	8.9	11.6
Autoclave operating conditions				
Pressure	kPa(g)	1050	1050	1050
Temperature – compartment 1	°C	141.9	143.9	145.2
Temperature – compartment 2	°C	144.5	148.1	149.2
Temperature – compartment 3	°C	145.1	146.9	148.4
Temperature – compartment 4	°C	147.2	144.9	146.9
Gas flowrates				
Enriched air oxygen concentration	%	28.12	34	30.8
Enriched air – compartment 1	Nm^3/hr	3100	2800	2689
Enriched air – compartment 2	Nm^3/hr	1100	1005	1053
Compressed air – compartment 3	Nm^3/hr	850	600	607
Compressed air – compartment 4	Nm^3/hr	500	600	608
Oxygen consumption				
Off-gas oxygen concentration	%	14.32	21.6	19.6

The plant trials only record the total recovery per autoclave and not recovery per leach stage/compartment as accurate sampling of each leach stage is difficult. A comparison of the copper extractions is shown in Table 10.

Table 10 – Comparison of Plant Results to Model Results

		Trial 1	Trial 2a	Trial 2b
Copper Extraction - actual	%	98.5	87.4	82.3
Copper Extraction – STM	%	94.22	87.10	82.03
Copper Extraction – NSM	%	95.45	87.74	82.79
Difference between STM and NSM	%	1.2%	0.7%	0.9%
Difference between models and actual	%	4.3%	0.4%	0.6%

The agreement between the 2 models is close and ranges between 0.7-1.2% for the three sets of data analysed. The STM uses far simpler mathematical techniques than the NSM, and takes a shorter period of time to solve.

The agreement between the models and the actual plant data ranges from 0.4-4.3%. The 2009 plant data recoveries were calculated from copper in solution values and based on the premise that the evaporation rate in the autoclaves is 10% of the solution feeding the compartment and the copper concentration in the spillage (approximately 5m³/hr of spillage is added to the autoclaves) is 10g/l. These values can in fact range between 5-15% for the evaporation rate and 5-30g/l for the spillage concentration [45], however the model correlation seems to indicate that the assumption is fair.

5.3 RRSB vs. Actual PSD

The NSM was used to calculate the difference in recovery obtained when the bimodal PSD of the 2009 data (from Trial 2a) was approximated with a RRSB distribution, compared to that obtained when the raw data was calculated with cubic spline interpolation. The overall recovery shown in Table 11 is 3% higher when the RRSB distribution is used, as it fails to accurately account for the second peak of coarser material apparent in the feed distribution. This subset of coarser material takes longer to react, as the particles are larger and hence it is logical that the lower recovery calculated when the actual PSD is used is correct, and that the RRSB approximation gives a falsely elevated recovery.

Table 11 – Difference in Recovery between Actual PSD and RRSB Approximation

Method	Cumulative Copper Recovery (%)			
	Compartment 1	Compartment 2	Compartment 3	Compartment 4
RRSB	52.22	66.71	77.39	89.84
Actual PSD via cubic spline interpolation	50.39	64.83	75.42	86.84

This exercise highlights the importance of using actual data where possible, instead of automatically resorting to well-known approximations (like the RRSB for PSD approximations) when devising a mathematical model.

5.4 Effect of Number of Simpson's Intervals for NSM

The NSM model uses Simpson's method to solve the integral. A simple test was completed to determine the effect of 100 intervals versus 1000 intervals. The comparison (as listed in Table 12) shows that 100 steps are sufficient.

Table 12 – Comparison of NSM Model Results using 2 Different Intervals

Method	Cumulative Copper Recovery (%)			
	Compartment 1	Compartment 2	Compartment 3	Compartment 4
NSM (1000 Simpson's intervals)	50.09	64.48	75.04	86.45
NSM (100 Simpson's intervals)	50.39	64.83	75.42	86.84

5.5 Actual PSD versus Modeled PSD

As leaching occurs through the 4 stages in the reactor, the PSD is expected to change. Larger particles leach into smaller size classes and smaller particles leach completely into solution. In an attempt to determine the actual PSD per leach stage, samples were taken from each leach compartment during the 2009 2a plant trial. These are shown graphically below in Figure 33. The feed PSD is shown in blue. The size distribution seems to show a bimodal characteristic in compartments 2 and 3, with a coarser fraction apparent at around 70 micron, but compartments 1 and 4 show a flatter PSD, with no bimodal characteristics.

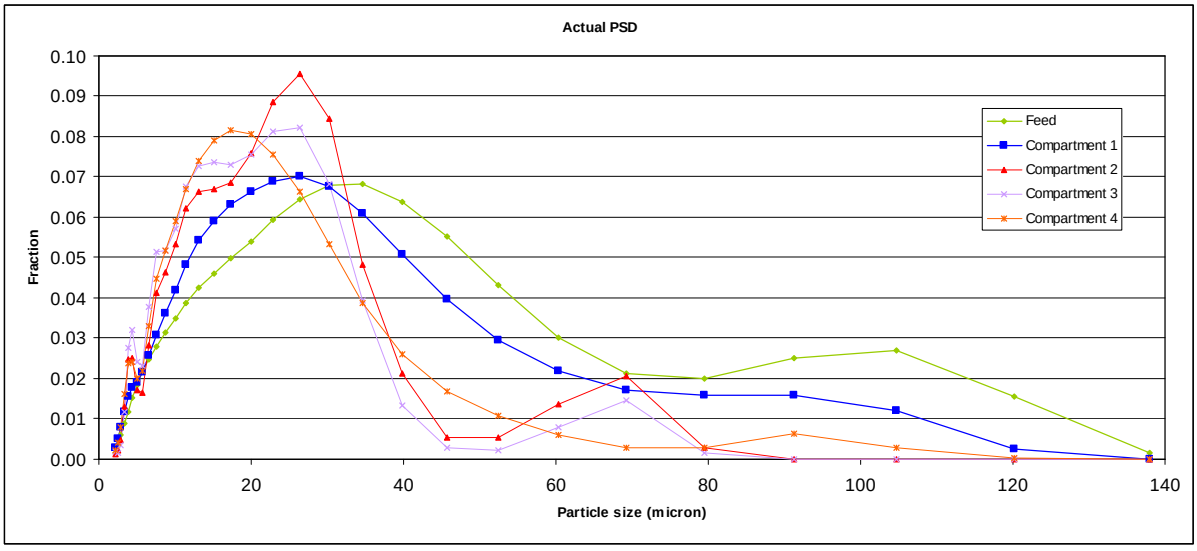

Figure 33 – Actual PSD across the 4 Dual Autoclave Compartments

The PSDs obtained from the 2 leach models for each of the 4 leach compartments are shown in Figure 34, Figure 35, Figure 36 and Figure 37.

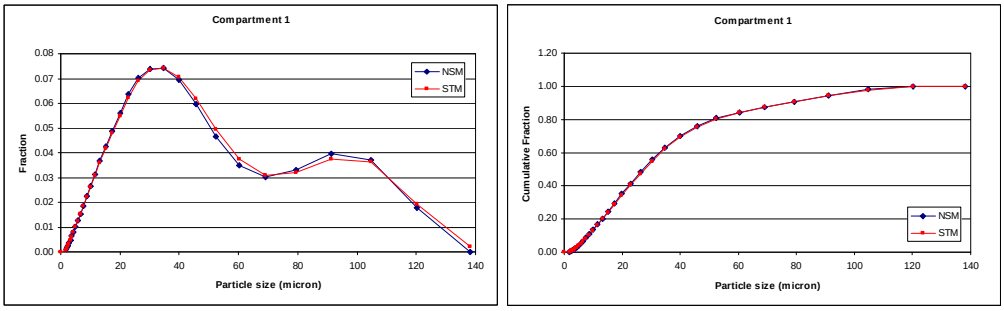

Figure 34 – PSD Graphs for the Solids Exiting Compartment 1

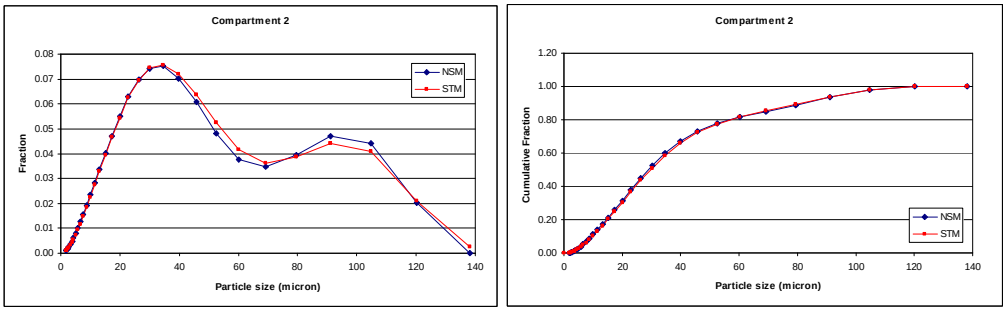

Figure 35 – PSD Graphs for the Solids Exiting Compartment 2

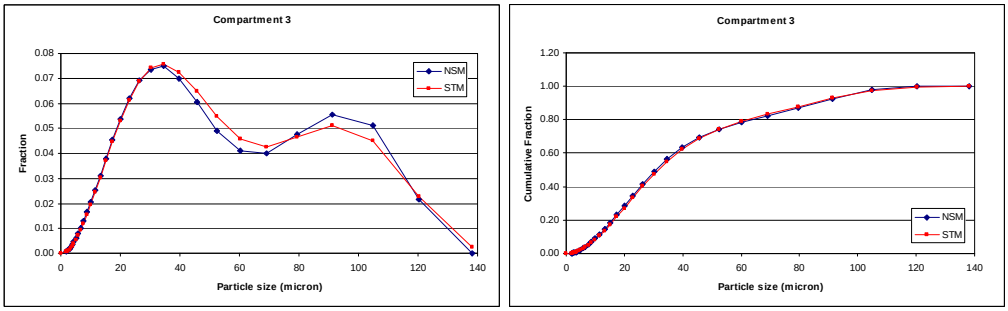

Figure 36 – PSD Graphs for the Solids Exiting Compartment 3

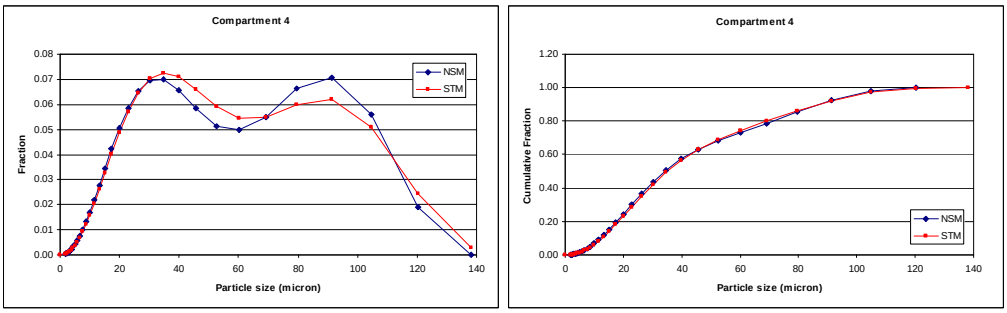

Figure 37 – PSD Graphs for the Solids Exiting Compartment 4

Compiling the above information onto a single set of axes results in a slightly noisy graph, but allows the changing predicted PSD as the leach progresses through the 4 stages to be observed.

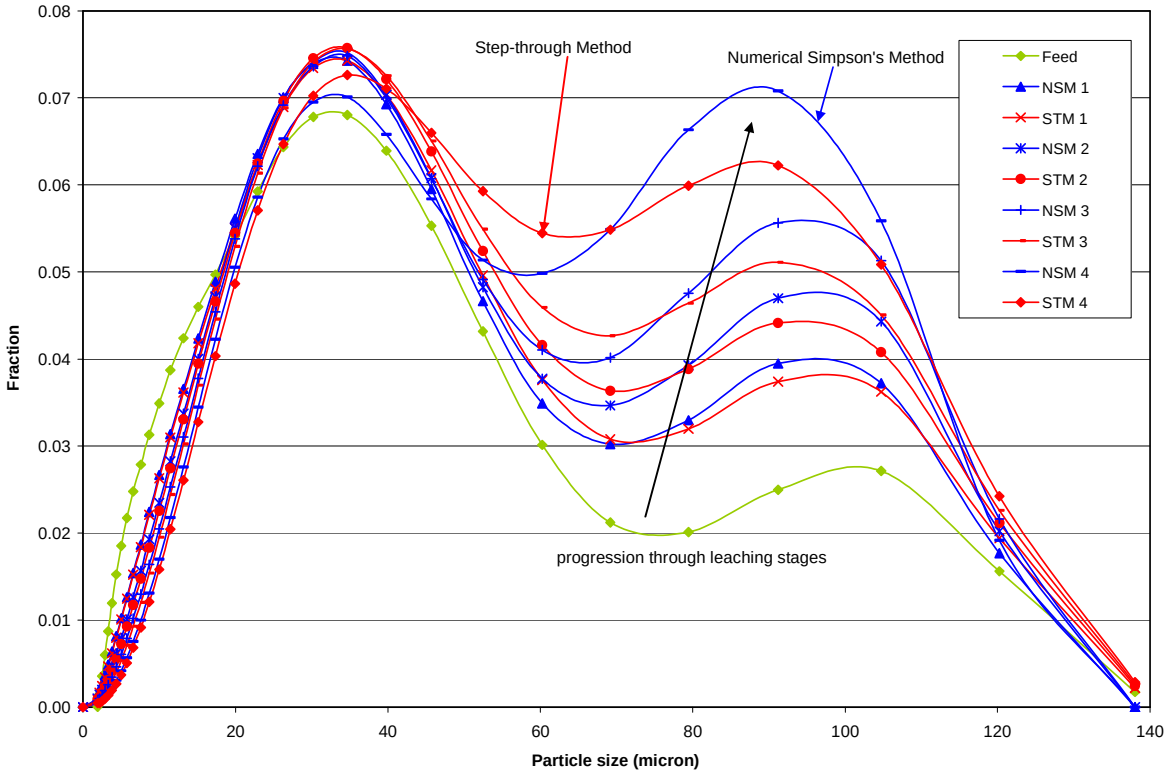

Figure 38 – Summary of Modeled Particle Size Changes through the Autoclave

A marked shift is noticed toward a coarser mean particle size (depicted using the arrow on the graph) as the leach progresses. The mean particle size per leach stage was calculated, as shown in Table 13.

Table 13 – Average Particle Size per Leach Compartment

Source	Average Particle Size (micron)				
	Feed	Compartment 1	Compartment 2	Compartment 3	Compartment 4
NSM model	31.9	36.9	39.5	42.1	45.6
STM model	31.9	37.3	39.9	42.3	46.0

The PSD curves for each stage move toward the coarser size fraction as flow progresses down the autoclave compartments. Sepulveda [13] notes this and attributes it partly to the fact that, under similar leaching constraints, fine particles react faster than coarse particles, because of their larger specific surface area and partly because certain particles react completely and thus do not form part of the particle accounting process. A possible reason for the disparity between the PSD of the plant samples compared to those attained with the model is that the plant samples were taken as grab samples and due to

the difficulties associated with obtaining a representative solid sample in a high pressure autoclave (which includes ensuring the 1.5m long dip-tube is line is flushed and vented properly before sampling, and taking a sufficient volume of sample). Hence the plant samples are possibly not representative.

5.6 Plant Troubleshooting with the Model

As mentioned in Section 2, part of the reason for developing a model is to try and assist with troubleshooting on the BMR. An attempt was made to try and explain why the plant copper recoveries (measured during 2009 and resulting in the plant audit) of ~85% are substantially lower than those reported by Hofirek [1], and historically attained in the plant. Two obvious differences in the plant were noticed, firstly the anomaly of the bimodal PSD and secondly the agitator configuration.

To test the hypothesis that the bimodal PSD negatively affects the recovery in the autoclaves, plant data from Trial 2a was inserted into the NSM and STM models with the bimodal PSD replaced with a more normal, unimodal PSD with a d95 of -45 micron.

Table 14 – Comparison of the Effect of a Coarse Bimodal PSD to a Normal PSD

Method	Cumulative Copper Recovery (%)			
	Compartment 1	Compartment 2	Compartment 3	Compartment 4
Trial 2a with bimodal PSD	52.06	65.76	76.09	87.74
Trial 2a with unimodal PSD, d95 -45micron	51.00	65.38	75.73	87.64

No significant difference is noted between the two recoveries and the hypothesis therefore needs to be rejected.

To test the hypothesis that the agitator configuration affects the recovery, Plant data from Trial 2a was inserted into the NSM and STM models with an agitator configuration of A-A-A-A and R-R-A-A instead of R-A-A-R. Rushton agitators have a greater power number than A315s and so are expected to exhibit far superior gas dispersion when utilised in the first two compartments of the autoclave, where most of the oxidation occurs. This is shown in Table 15.

Table 15 – Comparison of the Effect of Agitator Configuration

Method	Cumulative Copper Recovery (%)			
	Compartment 1	Compartment 2	Compartment 3	Compartment 4
Trial 2a with R-A-A-R	52.06	65.76	76.09	87.74
Trial 2a with A-A-A-A	24.29	37.86	48.22	55.07
Trial 2a with R-R-A-A	52.06	79.41	89.46	95.39

These calculations are based on the power numbers given to both the A315 and the Rushton's in literature and show that by altering the agitator configuration to R-R-A-A, the recovery should improve by ~8%. They also show that by changing the agitator configuration to A-A-A-A, the recovery shows a marked drop. The actual copper recovery for an A-A-A-A configuration (measured on one of the existing secondary autoclaves) was 83.6% [42], which is far greater than the models predicted 55.07%. This difference requires further investigation. Nonetheless the modeling approach has clearly shown that changing agitator configuration has a significant effect on leach recovery, which further supports its intended use as a diagnostic tool.

6 CONCLUSIONS

The aim of this project was to use fundamental data in the form of batch leach results, equipment specifications, process conditions and feed material characteristics to develop a simple but useful Excel model to approximate the secondary leach in the BMR, and then to use the model to determine whether the bimodal PSD or agitator configuration were responsible for the low leach efficiencies noted in the plant. After a considerable literature research in which different models were reviewed it was decided to use the Population Balance Model as the basis for the project.

The interpretation of batch leach data for a continuous, full-scale plant operation is not trivial. The model inputs (such as mineralogy and chemical reactions) are less well known than one would expect and therefore the determination of appropriate inputs and selection of plausible assumptions was an important part of the project. The initial assumptions made regarding the copper stoichiometry (by assuming stoichiometry associated with chalcocite and covellite) in setting up the leach model basics are a reasonable approximation based on the fact that the copper recoveries calculated in the models are within 0.4-4.3% of those measured in the plant.

Of particular interest is the discovery that the commonly used RRSB size distribution model is not always suitable, as shown in the case when a bimodal PSD is apparent. In this instance it would be better to use actual data or a cubic spline interpolation fit to actual data to provide an accurate equation describing the PSD, as the RRSB predicts a falsely elevated recovery.

The 2009 plant data used for the model development exhibited a bimodal PSD, with a coarse top-fraction. This coarse top-fraction was ultimately thought to contribute to the lower than expected copper recoveries in the plant. By replacing this PSD with a normal one (with a d95 -45 micron) in the model, there was no real change in the copper recovery. This requires further investigation because intuitively the coarse fraction should react more slowly. However, because the linear shrinkage rate of small and large particles is assumed to be constant in this model, this means the total amount of copper reacting remains the same, regardless of the PSD. All that happens is that the final product comprises a coarse fraction and the average particle size coarsens as the leach progresses (as shown and discussed in Section 5.5).

By changing the agitator configuration from R-A-A-R to R-R-A-A the predicted recovery improved from 87.74% to 95.39%. This is based on the power numbers given to both the A315 and the Rushtons in literature. Thus indications are that the agitator type (Rushton or A315) and configuration do affect the copper recovery significantly, and the effect is especially noticeable in the first 2 compartments of the autoclave as this is where approximately 75% of the gaseous reagent is added and most of the reaction occurs.

Thus, with regards to the effect of PSD and agitator configuration contributing to the reduced leach efficiency in the plant the bimodal PSD is not significantly responsible but the agitator configuration has a definitive effect.

The Numerical Simpson's Method and the Step-Through Method solve the population balance model using 2 very different methodologies to give results within 0.7-1.2% of each other. Results from the 3 plant trial data sets indicate that both methods can describe the effect on the secondary leach of:

- Throughput;
- Feed PSD;
- Oxygen addition rate;
- Temperature; and
- Agitator configuration.

The STM model is proposed as the more useful model for this application as it is a simpler method that is quicker to solve and in addition:

- It relies on no numerical techniques to solve;
- The method of stepping through the differential equation is simple and easy to understand and use; and
- The actual PSD is used (as long as it is a sufficiently detailed PSD and not just several points).

The models were successful in predicting recoveries using data from the 3 plant trials, however it must be noted that if further accuracy is required then the following steps are recommended:

The discrepancies in mineralogy noticed over the years should be investigated, and the quantification of minerals studied further. The benefit of setting up a database of feed material mineralogy to the secondary leach would be invaluable to allow the model to be developed further, as it would allow the feed characteristics to be more accurately defined and enable the inclusion of additional chemical reactions in the model with more confidence.

The chemical reactions used in the model should be further investigated, particularly considering the second stage of the batch leaching noticed in the Anglo batch data. Although the implications and possible effect of this second stage was disregarded in this report (as it was not clear why the Sherritt data did not exhibit a similar 2-stage curve and the inflection point occurred at ~90% copper recovery) the Anglo tests were conducted under extremely well-controlled conditions, which limits the possibility of experimental error contributing to the inflection point.

The formation of elemental sulphur in the autoclaves should possibly be accounted for as it does form under the leach conditions of the secondary autoclaves [2].

The performance of the A315 agitators needs to be investigated further. The calculated mass transfer coefficients for these agitators is around half that achieved with a Rushton, which does not agree with the performance noted by Hofirek in 1994 [1], or the plant in 2009 [42].

Representative information related to the PSD in each leach compartment must be obtained to compare to the modeled data and properly ascertain the effect of a coarse size fraction on the leach.

7 REFERENCES

1. Hofirek, Z., Nofal P. J., "Pressure Leach Capacity Expansion Using Oxygen-Enriched Air at RBMR (Pty) Ltd", Elsevier, Hydrometallurgy 39 (1995), 91-116.
2. Hofirek, Z., "Secondary Leach Residue (SLR) Production, Characterisation and Treatment", April 2001, Internal Anglo Platinum Report.
3. Peters, E., "The Mathematical Modeling of Leaching Systems", JOM, February 1991, Vol 43, No 2.
4. Nicol, M., "Hydrometallurgy, Theory and Practice, Study Guide 2008", Modules 5-6 presented at the UCT MSc lectures during 2008 – unpublished.
5. Safari, V., Arzpeyma, G., Rashchi, F., Mostoufi, N., "A Shrinking Particle-Shrinking Core Model for Leaching of a Zn Ore Containing Si", Int. Journal Miner. Process., 93 (2009)79-83.
6. Levenspiel, O., "The Chemical Reactor Omnibook", Oreg State Univ Bookstores, 1979, Section 5.
7. Crundwell, F., "Progress in the Mathematical Modeling of Leaching Reactors", Hydrometallurgy vol. 39, 1995, p 321-335.
8. Dreisinger, D., Dixon, D., "Hydrometallurgical Process Modelling for Design and Analysis Part 2: Leaching Kinetics and Associated Phenomena".
9. Dixon, D. G., "The Multiple Convolution Integral: A New Method for Modeling Multistage Continuous Leaching Reactors", Chemical Engineering Science, Vol 51, no. 21, p 4759-4767, 1996.
10. Kotsiopoulos, A., Hansford, G., Rawatlal, R., "An Approach to Segregation in Modeling Continuous Flow Tank Bioleach Systems", AIChE Journal, John Wiley and Sons, DOI 10.1002/aic.11479.
11. Hulbert, H., Katz, S., "Some Problems in Particle Technology – a Statistical-Mechanical Formulation", 19 (196) 555-574.
12. Randolph, A. D., "A Population Balance for Countable Entities", Canadian J Chem eng, 42, 280, 1964.
13. Sepulveda, J., Herbst, J., "A Population Balance Approach to the Modeling of Multistage Continuous Leaching Systems", The American Institute of Chemical Engineers Symposium Series, Fundamental Aspects of Hydrometallurgical Processes, Vol 74, No. 173, 1978, p41-65.
14. Crundwell, F. K., Bryson, A. W., "The Modelling of Particulate Leaching Reactors – the Population Balance Approach", Hydrometallurgy, vol 29, 1992, 275-295.

15. Dixon, D. G., "Improved Methods for the Design of Multistage Leaching Systems", Hydrometallurgy, 39 (1995) 337-351.
16. http://en.wikipedia.org/wiki/Henry's_law .
17. Tromans, D., "Temperature and Pressure Dependent Solubility of Oxygen in Water: a Thermodynamic Analysis", Hydrometallurgy, vol 48, 1998, 327-342.
18. Tromans, D., "Oxygen Solubility modeling in inorganic solutions: concentration, temperature and pressure effects", Hydrometallurgy, vol 50, 1998, 279-296, Elsevier.
19. http://en.wikipedia.org/wiki/Fick's_law_of_diffusion.
20. Kaskiala, T., "Studies in Gas-Liquid Mass Transfer in Atmospheric Leaching of Sulphide Zinc Concentrates", Doctoral thesis, Helsinki university of technology, Espoo 2005.
21. Pieterse, H., "Oxidation Autoclave Agitation Review", Pressure Hydrometallurgy 2004, METSOC, 34th Annual Hydrometallurgy meeting, 321-337.
22. Sip, A., Dembczynski, R., Juzuka, W., Czalzyk, K., Grajek, W., Jankowksi, T., "Scale-up of Divercin Production by Carnobacterium Divergens AS7 in Stirred Tank Reactors", Electronic Journal of Polish Agricultural Universities, Vol 11, Issue 1, 2008, www.ejpau.media.pl/volume11/issue1/art.04.html.
23. Moses, V., Springham, G., Cape, R. E., "Biotechnology: the Science and the Business", Harwood Academic Publishers, p191.
24. Meier, M., John, E., Wieckhusen, D., Wirth, W., Peukert, W., "Generally Applicable Breakage Functions Derived from Single Particle Comminution Data", Elsevier, Powder Technology 194 (2009) 33-41.
25. Mao, M.H., Peters, E., "Acid Pressure Leaching of Chalcocite", Proceedings of the 3rd international symposium on Hydrometallurgy, 1983, p243-260.
26. Velardo, A., Giona, M., Androver, A., Pagnanelli, F., Toro, L., "2-layer Shrinking Core Model: Parameter Estimation for the Reaction Order in Leaching Processes", Chem Eng Journal, 90 (2002), 231-240.
27. Kreyzig, E., "Advanced Engineering Mathematics", 6th Edition, p27-36; p481.
28. Kumar, J., Peglow, M., Warnecke, G., Heinrich, S., "An Efficient Numerical Technique for Solving Population Balance Equation involving Aggregation, Breakage, Growth and Nucleation", Elsevier, Powder Technology 182 (2008) 81-104
29. Kreyzig, E., "Advanced Engineering Mathematics", Wiley, 6th Edition, p266.
30. http://en.wikipedia.org/wiki/Dirac_delta_function.
31. Dimotakis, "The Kronecker and Dirac Delta Functions", 9 Nov 2002 http://www.its.caltech.edu/~aero101/AxB_Delta_021109.pdf.
32. Perry, R. H., Green, D., "Perry's Chemical Engineer's Handbook", 6th Edition, McGraw-Hill, Section 20-5.

33. Kreyzig, E., "Advanced Engineering Mathematics", Wiley, 6th Edition, p481.
34. Dynatec Corporation, Metallurgical Technologies Division, Rustenburg BMR Expansion, Hydrometallurgical Testwork, Vol. 1, March 2006, Fort Saskatchewan, Alberta, Canada, Section 6-34.
35. Levenspiel, O., "Chemical Reaction Engineering", 2nd edition, John Wiley and Sons, Ch 12.
36. Crundwell, F., "The Performance of Process Options for the Primary Copper Leach Autoclave", 22 February 2005 (Confidential company report).
37. Homma, S., Ogata, S., Koga, J., Matsumoto, S., "Gas-Solid Reaction Model for a Shrinking Spherical Particle with Unreacted Shrinking Core", Chemical Engineering Science 60 (2005), Elsevier, 4971-4980, 25 March 2005.
38. Paetz, J., "Report M/97/43 – Mineralogical Examination of PLR's associated with Process Difficulties (RBMR)", July 1996, unpublished internal report.
39. Dinham, P., Report M/06/11 – "Mineralogical Study of Leach Residues from the Dynatec Pilot Plant Trial", July 2006, unpublished internal report.
40. Dinham, P., Memo 09/67 – "Mineralogy of Primary Pressure Leach Repulp and Secondary Pressure Leach Compartment 4 Residue ex BMR, RBMR", May 2009, unpublished internal report.
41. E-mail correspondence with Petra Dinham, Senior Mineralogist at Anglo American
42. AGDP Course, Report Titled "BMR Secondary Autoclave Leaching Plant Trial" 2009, presented by Crundwell, F., Bryson, L. J., internal report, unpublished.
43. Kruger, C. J. C., "Constrained Cubic Spline Interpolation for Chemical Engineering Applications", http://www.korf.co.uk/spline.pdf.
44. Kreyzig, E. "Advanced Engineering Mathematics", Wiley, 6th Edition, p981-983.
45. E-mail correspondence with JJ Taute, Senior Metallurgist at the BMR

8 APPENDICES

8.1 Appendix 1

Sherrit Gordon Batch Test Summary

BATCH TEST 6

Temperature		℃	140
Pressure	Water vapour	bar	3.59
	Total autoclave	kPa	703.7214626
	Total autoclave	bar	6.95
	Enriched air	bar	3.36
Oxygen	Pressure	bar	3.36
	Solubility	mol/L	0.00297
		mol/m³	2.97417
	Enrichment		100%

Time	Cu_2S Extr %
0	0.00
1800	68.90
3600	90.00
5400	96.20
7200	100.00
10800	100.00
14400	100.00

BATCH TEST 7

Temperature		℃	130
Pressure	Water vapour	bar	2.69
	Total autoclave	kPa	612.2670676
	Total autoclave	bar	6.04
	Enriched air	bar	3.36
Oxygen	Pressure	bar	3.36
	Solubility	mol/L	0.00283
		mol/m³	2.83404
	Enrichment		100%

	Time	Cu_2S Extr %
0	0	0.00
30	1800	54.00
60	3600	73.70
90	5400	85.30
120	7200	91.40
180	10800	100.00
240	14400	100.00

BATCH TEST 8

Temperature		℃	150
Pressure	Water vapour	bar	4.73
	Total autoclave	kPa	818.8132229
	Total autoclave	bar	8.08
	Enriched air	bar	3.36
Oxygen	Pressure	bar	3.36
	Solubility	mol/L	0.00315
		mol/m³	3.14977
	Enrichment		100%

Time	Cu_2S Extr %
0	0.00
1800	85.20
3600	97.10
5400	100.00
7200	100.00
10800	100.00
14400	100.00

BATCH TEST 9

Temperature		℃	140
Pressure	Water vapour	bar	3.59
	Total autoclave	kPa	503.7214626
	Total autoclave	bar	4.97
	Enriched air	bar	1.38
Oxygen	Pressure	bar	1.38
	Solubility	mol/L	0.00122
		mol/m³	1.22466
	Enrichment		100%

Time	Cu_2S Extr %
0	0.00
1800	53.90
3600	77.00
5400	89.40
7200	94.30
10800	100.00
14400	100.00

BATCH TEST 10

Temperature		℃	140
Pressure	Water vapour	bar	3.59
	Total autoclave	kPa	903.7214626
	Total autoclave	bar	8.92
	Enriched air	bar	5.33
Oxygen	Pressure	bar	5.33
	Solubility	mol/L	0.00472
		mol/m³	4.72368
	Enrichment		100%

Time	Cu_2S Extr %
0	0.00
1800	77.50
3600	94.20
5400	100.00
7200	100.00
10800	100.00
14400	100.00

8.2 Appendix 2

Anglo Research Batch Test Data Summary

BATCH TEST 1

Temperature		℃	160
Pressure	Water vapour	bar	6.14
	Total autoclave	kPa	800
	Total autoclave	bar	7.90
	Enriched air	bar	1.76
Oxygen	Pressure	bar	1.76
	Solubility	mol/L	0.00176
		mol/m³	1.76250
	Enrichment		100%

Time	Cu Extr (X) %
0	19.08
300	46.35
600	68.65
900	88.85
1200	95.17
1500	97.18
1800	97.56
2700	99.34

BATCH TEST 2

Temperature		℃	145
Pressure	Water vapour	bar	4.13
	Total autoclave	kPa	600
	Total autoclave	bar	5.92
	Enriched air	bar	1.80
Oxygen	Pressure	bar	1.80
	Solubility	mol/L	0.00164
		mol/m³	1.63612
	Enrichment		100%

Time	Cu Extr %
0	17.21
300	35.54
600	46.60
900	58.30
1200	66.73
1500	73.92
1800	78.66
2700	88.56
3600	91.44
4500	93.41
5400	94.35
7200	96.99
8100	99.00

BATCH TEST 3

Temperature		℃	120
Pressure	Water vapour	bar	1.98
	Total autoclave	kPa	400
	Total autoclave	bar	3.95
	Enriched air	bar	1.97
Oxygen	Pressure	bar	1.97
	Solubility	mol/L	0.00160
		mol/m³	1.60001
	Enrichment		100%

Time	Cu_2S Extr %
0	17.94
300	34.77
600	44.72
900	52.37
1200	60.66
1500	66.09
1800	70.54
2700	81.20
3600	89.71
4500	92.00
5400	93.10
6300	93.70
7200	94.24
8100	95.04

BATCH TEST 4

Temperature		℃	145
Pressure	Water vapour	bar	4.13
	Total autoclave	kPa	468.7179705
	Total autoclave	bar	4.63
	Enriched air	bar	0.50
Oxygen	Pressure	bar	0.50
	Solubility	mol/L	0.00046
		mol/m³	0.45558
	Enrichment		100%

Time	Cu_2S Extr %
0	15.00
300	28.28
600	34.99
900	42.84
1200	50.84
1500	60.13
1800	67.14
2700	82.17
3600	91.19
4500	92.19
5400	94.49
7200	96.90
8100	98.00
9000	99.11
9900	99.91

BATCH TEST 5

Temperature		℃	145
Pressure	Water vapour	bar	4.13
	Total autoclave	kPa	823.35547
	Total autoclave	bar	8.13
	Enriched air	bar	4.00
Oxygen	Pressure	bar	4.00
	Solubility	mol/L	0.00364
		mol/m³	3.64463
	Enrichment		100%

Time	Cu extr (X) %
0	13.81
300	44.67
600	67.24
900	83.72
1200	88.62
1500	91.03
2700	92.98
5400	94.27
7200	96.89
9000	97.23
9900	98.66
11700	99.85

8.3 Appendix 3

ARRHENIUS

		same Co2	
T	ks'	[Co2]s	A
K		mol/m³	
433.15	5.83E-04	1.76250	77.20607125
418.15	2.01E-04	1.63612	80.25840859
393.15	1.49E-04	1.60001	81.19740947
		1.66621	**79.5539631**

y	x
ln(ks')	1/T
-7.447244726	0.002308669
-8.51093621	0.002391486
-8.813243491	0.002543558

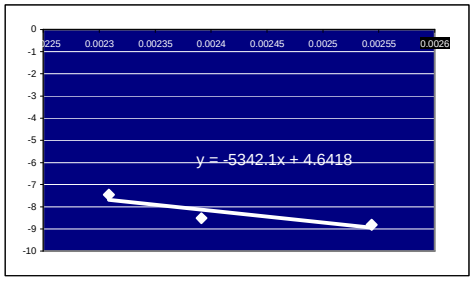

slope	-5342.13	-Ea/R
intercept	4.641808563	= ln(A)+nln(CO2)
Ea	44414.45656	J/mol.K
ln(A. CO2^n)	4.641808563	

CALCULATE "n"

same temp

T	ks'	[Co2]s
K		mol/m³
418.15	2.01E-04	1.63612
418.15	1.67E-04	0.45558
418.15	5.36E-04	3.64463

y	x
ln(ks')	ln[Co2]s
-8.51093621	0.492328471
-8.694742944	-0.786187395
-7.531133484	1.293254147

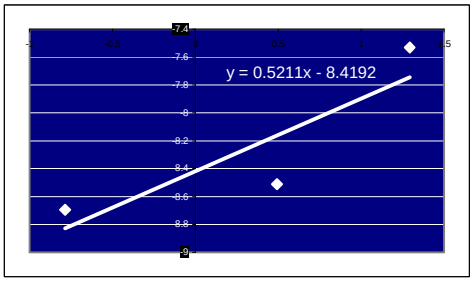

slope	0.52	n
intercept	-8.419202316	

8.4 Appendix 4

Secondary Feed Material PSD

Sample Name:	DC1	**Measured:**	Wednesday 8 April 2009
		Analyst:	Summerton, GC Dr
Dispersant:	Water	**Obscuration:**	13.20%
Weighted Residual:	1.76%		
d(0.1):	6.188µm	**Pump Speed:**	2000 rpm
d(0.5):	23.093µm		
d(0.9)	64.374µm		

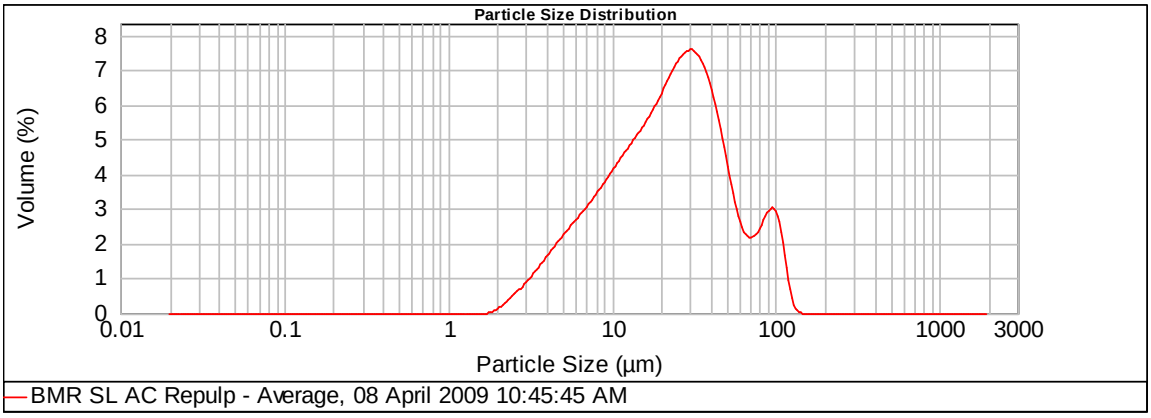

Size (µm)	Vol Under %	Size (µm)	Vol Under %	Size (µm)	Vol Under %	Size (µm)	Vol Under %	Size (µm)	Vol Under %	Size (µm)	Vol Under %
0.010	0.00	0.105	0.00	1.096	0.00	11.482	24.49	120.226	99.83	1258.925	100.00
0.011	0.00	0.120	0.00	1.259	0.00	13.183	28.73	138.038	100.00	1445.440	100.00
0.013	0.00	0.138	0.00	1.445	0.00	15.136	33.33	158.489	100.00	1659.587	100.00
0.015	0.00	0.158	0.00	1.660	0.00	17.378	38.30	181.970	100.00	1905.461	100.00
0.017	0.00	0.182	0.00	1.905	0.00	19.953	43.71	208.930	100.00	2187.762	100.00
0.020	0.00	0.209	0.00	2.188	0.16	22.909	49.64	239.883	100.00	2511.886	100.00
0.023	0.00	0.240	0.00	2.512	0.51	26.303	56.07	275.423	100.00	2884.032	100.00
0.026	0.00	0.275	0.00	2.884	1.11	30.200	62.85	316.228	100.00	3311.311	100.00
0.030	0.00	0.316	0.00	3.311	1.99	34.674	69.66	363.078	100.00	3801.894	100.00
0.035	0.00	0.363	0.00	3.802	3.18	39.811	76.05	416.869	100.00	4365.158	100.00
0.040	0.00	0.417	0.00	4.365	4.71	45.709	81.58	478.630	100.00	5011.872	100.00
0.046	0.00	0.479	0.00	5.012	6.56	52.481	85.90	549.541	100.00	5754.399	100.00
0.052	0.00	0.550	0.00	5.754	8.74	60.256	88.92	630.957	100.00	6606.934	100.00
0.060	0.00	0.631	0.00	6.607	11.21	69.183	91.04	724.436	100.00	7585.776	100.00
0.069	0.00	0.724	0.00	7.586	14.00	79.433	93.05	831.764	100.00	8709.636	100.00
0.079	0.00	0.832	0.00	8.710	17.13	91.201	95.55	954.993	100.00	10000.000	100.00
0.091	0.00	0.955	0.00	10.000	20.62	104.713	98.26	1096.478	100.00		

8.5 Appendix 5

Code for Simpson's Integral and Cubic Spline Interpolation [41]

```
Function SimpsonInt(A As Double, B As Double, ByVal N As Long, k As Double, l As
Double, w As Double, metode As Integer, xx As Range, yy As Range, z As Double) As
Double
' Returns the integral of Func (below) from a to b using Composite Simpson's Rule over n
intervals
    Dim i       As Double  ' index
    Dim dH      As Double  ' step size
    Dim dOdd    As Double  ' sum of Func(i), i = 1, 3, 5, 7, ... n-1, i.e., n/2 values
    Dim dEvn    As Double  ' sum of Func(i), i =   2, 4, 6,  ... n-2  i.e., n/2 - 1 values
    ' 1 + (n/2) + (n/2 - 1) + 1 = n+1 function evaluations
    If N < 1 Then Exit Function
    If N And 1 Then N = N + 1 ' n must be even
    dH = (B - A) / N
    For i = 1 To N - 1 Step 2
        dOdd = dOdd + Func(A + i * dH, k, l, w, metode, xx, yy, z)

    Next
    For i = 2 To N - 2 Step 2
        dEvn = dEvn + Func(A + i * dH, k, l, w, metode, xx, yy, z)
    Next
    SimpsonInt = ((0.5 * Func(A, k, l, w, metode, xx, yy, z)) + 4# * dOdd + 2# * dEvn
+ (0.5 * Func(B, k, l, w, metode, xx, yy, z))) * dH / 3# ' weighted sum
End Function

Function Func(xi As Double, k As Double, l As Double, w As Double, metode As Integer,
xx As Range, yy As Range, z As Double) As Double

    ' replace this function with the function to be integrated

    Func = (-k * cubspline(metode, xi, xx, yy) * Exp((l - xi) / (z * w)) * (l / xi) ^ 3)

End Function
Function cubspline(metode As Integer, xi As Double, xx As Object, yy As Object) As
Double

Dim i As Integer
Dim yi As Double
Dim x() As Double
Dim y() As Double
Dim y2() As Double
Dim j As Integer

If metode = 1 Then
  'Numerical Recipes are 1 based
  j = 0
Else
  'Others are 0 based
```

```
  j = -1
End If

For i = 1 To UBound(xx())
  If yy(i) <> "" Then
    j = j + 1
    ReDim Preserve x(j)
    ReDim Preserve y(j)
    x(j) = CDbl(xx(i))
    y(j) = CDbl(yy(i))
  End If
Next i

If metode = 1 Then
  'NR cubic spline
  'Get y2
  ReDim y2(1 To UBound(x()))
  Call spline(x(), y(), UBound(x()), 10 ^ 30, 10 ^ 30, y2())
  'Get y
  Call splint(x(), y(), y2(), UBound(x()), xi, yi)
ElseIf metode = 3 Then
  'Own cubic spline
  yi = SplineX3(xi, x(), y())
End If

'Return
cubspline = yi

End Function

Sub spline(x() As Double, y() As Double, N As Integer, yp1 As Double, ypn As Double,
y2() As Double)

'Given arrays x(1:n) and y(1:n) containing a tabulated function, i.e., y i = f(xi), with
'x1<x2< :::<xN , and given values yp1 and ypn for the first derivative of the inter-
'polating function at points 1 and n, respectively, this routine returns an array y2(1:n) of
'length n which contains the second derivatives of the interpolating function at the
tabulated
'points xi. If yp1 and/or ypn are equal to 1 * 10^30 or larger, the routine is signaled to
set
'the corresponding boundary condition for a natural spline, with zero second derivative on
'that boundary.
'Parameter: NMAX is the largest anticipated value of n.

    Dim Nmax As Integer
    Nmax = 500

    Dim i As Integer
    Dim k As Integer

    Dim p As Double
    Dim qn As Double
    Dim sig As Double
    Dim un As Double
```

```
    ReDim u(Nmax) As Double

    'The lower boundary condition is set either to be natural
    If (yp1 > 9.9E+29) Then
      y2(1) = 0#
      u(1) = 0#
    Else
      'or else to have a specicied first derivative.
      y2(1) = -0.5
      u(1) = (3# / (x(2) - x(1))) * ((y(2) - y(1)) / (x(2) - x(1)) - yp1)
    End If

    'This is the decomposition loop of the tridiagonal
    'algorithm. y2 and u are used for temporary
    'storage of the decomposed factors.

    For i = 2 To N - 1
      sig = (x(i) - x(i - 1)) / (x(i + 1) - x(i - 1))
      p = sig * y2(i - 1) + 2#
      y2(i) = (sig - 1#) / p
      u(i) = (6# * ((y(i + 1) - y(i)) / (x(i + 1) - x(i)) - (y(i) - y(i - 1)) / (x(i) - x(i - 1)))
/ (x(i + 1) - x(i - 1)) - sig * u(i - 1)) / p
    Next i

    'The upper boundary condition is set either to be natural
    If (ypn > 9.9E+29) Then
      qn = 0#
      un = 0#
    Else
      'or else to have a specified first derivative.
      qn = 0.5
      un = (3# / (x(N) - x(N - 1))) * (ypn - (y(N) - y(N - 1)) / (x(N) - x(N - 1)))
    End If
    y2(N) = (un - qn * u(N - 1)) / (qn * y2(N - 1) + 1#)

    'This is the backsubstitution loop of the tridiagonal algorithm.
    For k = N - 1 To 1 Step -1
      y2(k) = y2(k) * y2(k + 1) + u(k)
    Next k

End Sub

Sub splint(xa() As Double, ya() As Double, y2a() As Double, N As Integer, x As Double,
y As Double)

'Given the arrays xa(1:n) and ya(1:n) of length n, which tabulate a function (with the
'xai 's in order), and given the array y2a(1:n), which is the output from spline above,
'and given a value of x, this routine returns a cubic-spline interpolated value y.

    Dim k As Integer
    Dim khi As Integer
    Dim klo As Integer

    Dim A As Double
```

```
    Dim B As Double
    Dim h As Double

    'We will the right place in the table by means of bisection.
    klo = 1
    khi = N

    While (khi - klo > 1)
      k = (khi + klo) / 2
      If (xa(k) > x) Then
        khi = k
      Else
        klo = k
      End If
    Wend

    'klo and khi now bracket the input value of x.
    h = xa(khi) - xa(klo)
    If (h = 0) Then MsgBox ("bad xa input in splint")

    'Cubic spline polynomial is now evaluated.
    A = (xa(khi) - x) / h
    B = (x - xa(klo)) / h
    y = A * ya(klo) + B * ya(khi) + ((A ^ 3 - A) * y2a(klo) + (B ^ 3 - B) * y2a(khi)) *
(h ^ 2) / 6#

End Sub

Public Function SplineX3(x As Double, xx() As Double, yy() As Double) As Double
'|-------------------------------------------------------------------------
'| Function returns y value for a corresponding x value, based on cubic spline.
'| Will never oscillates or overshoot. No need to solve matrix.
'| Also calculate constants for cubic in case needed (for integration).
'|
'| xx(0 to No_of_lines) is x values
'|    * Must be unique (no two consequetive ones the same)
'|    * Must be in ascending order
'|    * No of lines = Number of points - 1
'| yy(0 to No_of_lines) is y values
'|
'| Uses function dxx to prevent div by zero.
'|
'| Developer: C Kruger, Guildford, UK
'| Date: December 2001
'|-------------------------------------------------------------------------

Dim i As Integer
Dim j As Integer
Dim Nmax As Integer
Dim Num As Integer

'1st and 2nd derivative for left and right ends of line
Dim gxx(0 To 1) As Double
Dim ggxx(0 To 1) As Double
```

```
'Constants for cubic equations
Dim A As Double     'Also for linear extrapolation
Dim B As Double     'Also for linear extrapolation
Dim C As Double
Dim D As Double

'Number of lines = points - 1
Nmax = UBound(xx())

'(1a) Find LineNumber or segment. Linear extrapolate if outside range.
Num = 0
If x < xx(0) Or x > xx(Nmax) Then
  'X outisde range. Linear interpolate
  'Below min or max?
  If x < xx(0) Then Num = 1 Else Num = Nmax
  B = (yy(Num) - yy(Num - 1)) / dxx(xx(Num), xx(Num - 1))
  A = yy(Num) - B * xx(Num)
  SplineX3 = A + B * x
  Exit Function

'(1b) Find LineNumber or segment. Linear extrapolate if outside range.
Else
  'X in range. Get line.
  For i = 1 To Nmax
    If x <= xx(i) Then
      Num = i
      Exit For
    End If
  Next i
End If

'(2) Calc first derivative (slope) for intermediate points
For j = 0 To 1          'Two points around line
  i = Num - 1 + j
  If i = 0 Or i = Nmax Then
    'Set very large slope at ends
    gxx(j) = 10 ^ 30
  ElseIf (yy(i + 1) - yy(i) = 0) Or (yy(i) - yy(i - 1) = 0) Then
    'Only check for 0 dy. dx assumed NEVER equals 0 !
    gxx(j) = 0
  ElseIf ((xx(i + 1) - xx(i)) / (yy(i + 1) - yy(i)) + (xx(i) - xx(i - 1)) / (yy(i) - yy(i - 1))) =
0 Then
    'Pos PLUS neg slope is 0. Prevent div by zero.
    gxx(j) = 0
  ElseIf (yy(i + 1) - yy(i)) * (yy(i) - yy(i - 1)) < 0 Then
    'Pos AND neg slope, assume slope = 0 to prevent overshoot
    gxx(j) = 0
  Else
    'Calculate an average slope for point based on connecting lines
    gxx(j) = 2 / (dxx(xx(i + 1), xx(i)) / (yy(i + 1) - yy(i)) + dxx(xx(i), xx(i - 1)) / (yy(i)
- yy(i - 1)))
  End If
Next j
```

```
'(3) Reset first derivative (slope) at first and last point
If Num = 1 Then
  'First point has 0 2nd derivative
  gxx(0) = 3 / 2 * (yy(Num) - yy(Num - 1)) / dxx(xx(Num), xx(Num - 1)) - gxx(1) / 2
End If
If Num = Nmax Then
  'Last point has 0 2nd derivative
  gxx(1) = 3 / 2 * (yy(Num) - yy(Num - 1)) / dxx(xx(Num), xx(Num - 1)) - gxx(0) / 2
End If

'(4) Calc second derivative at points
ggxx(0) = -2 * (gxx(1) + 2 * gxx(0)) / dxx(xx(Num), xx(Num - 1)) + 6 * (yy(Num) -
yy(Num - 1)) / dxx(xx(Num), xx(Num - 1)) ^ 2
ggxx(1) = 2 * (2 * gxx(1) + gxx(0)) / dxx(xx(Num), xx(Num - 1)) - 6 * (yy(Num) -
yy(Num - 1)) / dxx(xx(Num), xx(Num - 1)) ^ 2

'(5) Calc constants for cubic
D = 1 / 6 * (ggxx(1) - ggxx(0)) / dxx(xx(Num), xx(Num - 1))
C = 1 / 2 * (xx(Num) * ggxx(0) - xx(Num - 1) * ggxx(1)) / dxx(xx(Num), xx(Num -
1))
B = (yy(Num) - yy(Num - 1) - C * (xx(Num) ^ 2 - xx(Num - 1) ^ 2) - D * (xx(Num) ^
3 - xx(Num - 1) ^ 3)) / dxx(xx(Num), xx(Num - 1))
A = yy(Num - 1) - B * xx(Num - 1) - C * xx(Num - 1) ^ 2 - D * xx(Num - 1) ^ 3

'Return function
SplineX3 = A + B * x + C * x ^ 2 + D * x ^ 3

''Alternative method based on Numerical Recipes.
''Shorter but does not calc cubic constants A, B, C, D
'i = Num
'A = (xx(i) - x) / (xx(i) - xx(i - 1))
'B = 1 - A
'Cy = 1 / 6 * (A ^ 3 - A) * (6 * (yy(i) - yy(i - 1)) - 2 * (gxx(i) + 2 * gxx(i - 1)) *
(xx(i) - xx(i - 1)))
'Dy = 1 / 6 * (B ^ 3 - B) * (2 * (2 * gxx(i) + gxx(i - 1)) * (xx(i) - xx(i - 1)) - 6 *
(yy(i) - yy(i - 1)))
''Return function
'SplineX3 = A * yy(i - 1) + B * yy(i) + Cy + Dy

End Function

Public Function dxx(x1 As Double, x0 As Double) As Double
'Calc Xi - Xi-1 to prevent div by zero

dxx = x1 - x0
If dxx = 0 Then dxx = 10 ^ 30

End Function
```